

# 1 Pacific Southern Ocean coccolithophore-estimated particulate 2 inorganic carbon (PIC) versus satellite-derived PIC measurements

3 Mariem Saavedra-Pellitero<sup>1</sup>, Karl-Heinz Baumann<sup>2</sup>, Nuria Bachiller-Jareno<sup>1</sup>, Harold Lovell<sup>1</sup>, Nele  
4 Manon Vollmar<sup>2,3</sup>, Elisa Malinverno<sup>4</sup>

5  
6 <sup>1</sup>School of the Environment, Geography and Geosciences, University of Portsmouth, Portsmouth, PO1 3QL, United Kingdom

7 <sup>2</sup>Department of Geosciences, University of Bremen, 28334, Bremen, Germany

8 <sup>3</sup>NORCE Norwegian Research Centre AS, NORCE Climate & Environment, 5007, Bergen, Norway and Bjerknes Centre for  
9 Climate Research, Bergen, Norway

10 <sup>4</sup>Department of Geological Sciences and Geotechnologies, Milano-Bicocca University, 20126, Milan, Italy

11

12 Correspondence to: Mariem Saavedra-Pellitero (mariem.saavedra-pellitero@port.ac.uk)

## 13 Abstract

14 Polar plankton communities are experiencing the impact of ocean acidification and global warming. Coccolithophores are the  
15 main type of calcifying phytoplankton in the Southern Ocean (SO) and they play a key role in the carbon cycle through the  
16 production of particulate organic, and inorganic carbon (PIC). However, in situ coccolithophore studies in the SO are sparse  
17 in space and time due to the harsh weather conditions. An alternative tool for monitoring PIC is the use of optical remote  
18 sensing, because coccolithophores account for most of the optical PIC backscattering in the sea. Here, we combine  
19 micropalaeontology and remote sensing to evaluate discrepancies between coccolithophore and satellite-derived PIC in the  
20 Pacific SO (in non-bloom conditions). Plankton samples were collected along two latitudinal transects: from New Zealand to  
21 Antarctica (December 2004-January 2005) and across the Drake Passage (February-March 2016). We compare PIC estimates  
22 derived from (1) Scanning Electron Microscope coccolith morphometric analyses and (2) MODIS-Aqua L2 and L3 PIC  
23 concentration values. In general, the coccolith-estimated PIC and satellite-derived PIC datasets show comparable trends in the  
24 Subantarctic and Polar Front Zones of both transects, with PIC-satellite values being generally higher than coccolith-derived  
25 PIC. However, satellite data availability was impacted by cloud cover in the SO. According to the coccolithophorid data,  
26 *Emiliania huxleyi* morphogroup B substantially contributes to the sea-surface PIC content south of the Subantarctic Front in  
27 both transects, whereas *E. huxleyi* type A, type A overcalcified, and other taxa (e.g. *Calcidiscus leptoporus*), only contribute  
28 to coccolithophore PIC in the northernmost stations. High satellite-derived PIC values south of the Polar Front, are not apparent  
29 in the coccolithophore data. We suggest that the high reflectance signal at the Antarctic Zone may instead relate to the presence  
30 of small biogenic opal particles (e.g. diatoms, silicoflagellates and/or small siliceous plankton) or other unknown highly  
31 reflective particles (such as *Phaeocystis* aggregations). Our results highlight the challenges presented by the lack of reliable

satellite data in some parts of the SO as well as the importance of in situ measurements and methodological accuracy when estimating PIC values. This work contributes to our understanding of coccolithophore PIC dynamics in the “data desert” of the vast Pacific SO, offering valuable insights into high-latitude phytoplankton and zooplankton communities.

## 1 Introduction

Coccolithophores are a major component of calcifying phytoplankton communities in the Southern Ocean (SO) (e.g. Saavedra-Pellitero et al., 2014; Saavedra-Pellitero et al., 2019; Malinverno et al., 2015; Charalampopoulou et al., 2016; Rigual Hernández et al., 2020a) and play an important and complex role in the carbon cycle through the production of particulate inorganic carbon (PIC) and particulate organic carbon (e.g. Rost and Riebesell, 2004; Salter et al., 2014). These haptophyte algae produce an external covering (coccosphere) of interlocking calcite platelets (coccoliths). This process decreases the alkalinity of surface waters, thereby reducing the uptake of CO<sub>2</sub> from the atmosphere into the surface ocean and thus acting in opposition to carbon sequestration by the biological carbon pump (Rost and Riebesell, 2004). Previous work has suggested that calcification during blooms of the coccolithophore *Emiliania huxleyi*, aka *Gephyrocapsa huxleyi* (Bendif et al., 2023), might alter the air-sea flux of CO<sub>2</sub> (e.g. Harlay et al., 2010; Shutler et al., 2013), although to date, the impact of this has mostly only been explored on a limited regional basis (e.g. Holligan et al., 1993; Robertson et al., 1994; Balch et al., 2016).

Since the early days of satellite-based color measurements of the oceans, large coccolithophore blooms have been visible as highly reflective regions in satellite images (e.g. Holligan et al., 1983). Coccolithophores, and their detached coccoliths, are strongly optically active and notably affect the optical budget of the surface ocean, and can thus be seen from space using satellite remote sensing (Smyth et al., 2002; Tyrrell and Taylor, 1996). Coccolithophores are responsible for most of the optical PIC backscatter in the ocean; the other, larger PIC particles associated with foraminifera and pteropods provide negligible backscatter per unit mass and therefore have minimal optical impact (Balch et al., 1996). In general, detached coccoliths account for 10-20% of the light backscattered from the sea under non-bloom conditions, whereas under bloom conditions it can be more than 90% (Balch et al., 1991; Balch et al., 1999). The strong scattering properties of the coccolithophores and the associated PIC lead to enhanced reflection in the entire visible spectrum (400-700 nm). Gordon et al. (2001) and Balch et al. (2005) developed algorithms to estimate the PIC concentration in the surface layer of the water column from the radiance emanating from the water. The relationship between inherent optical properties and the resultant light fields is well understood (e.g. Mitchell et al., 2017). The difficulty lies in understanding the combined effects of different in-water constituents on the inherent optical properties, and ultimately, the underwater light fields. While there have been many advances in this area (e.g. Babin et al., 2003a; Babin et al., 2003b; Devred et al., 2006), there will always be some uncertainty in calculating these relationships. For example, it has been shown that satellite ocean-color-based PIC estimates did not match in situ (ship-based)

observations and that satellite-derived PIC can be overestimated in Antarctic waters (e.g. Holligan et al., 2010; Trull et al., 2018). One potential source of error is that aquamarine waters characterized by high reflectance of light can also be caused by suspended sediment and even opal particles, such as fragments of diatom frustules (e.g. Broerse et al., 2003).

Satellite data has played a key role in showing the importance of the increasing *E. huxleyi* blooms in the world's oceans (e.g. Balch et al., 1991; Iida et al., 2002; Siegel et al., 2007; Neukermans et al., 2018; for further citations see the comprehensive review in Balch and Mitchell, 2023). This is relevant for monitoring changes at a global scale and to detect seasonal patterns as well as interannual variations (e.g. Smyth et al., 2004; Winter et al., 2014; Rigual-Hernández et al., 2020a) or trends, with the ultimate goal of feeding information into models for climate projections in the context of global warming and ocean acidification (e.g. Neukermans et al., 2018; Krumhardt et al., 2019). Recent concerns about climate change and ocean acidification pointed to *E. huxleyi* as a target cosmopolitan species to understand the biological response. Expansion or reduction of the biogeographic range, changes in coccolith calcification and preservation are possible responses that were observed in water and sediment samples. The high-latitude distribution of *E. huxleyi* has undergone a recent poleward expansion in both the northern (Rivero-Calle et al., 2015) and southern hemisphere (Cubillos et al., 2007; Winter et al., 2014). However, data from the SO is rather limited and there are currently not enough in situ measurements to unravel the complex dynamic relationships between *E. huxleyi* distribution and the frontal dynamics of the Antarctic Circumpolar Current (ACC). Significant zonal differences are shown in the relationship between coccolithophore data and ACC frontal positions across the different sectors of the SO (e.g. Saavedra-Pellitero et al., 2014), but no strong evidence of recent expansion on a circumpolar scale has been identified (Malinverno et al., 2015).

The band of high reflectance and elevated PIC waters observed in the SO between 30° - 60° S during Austral summer, known as “the Great Calcite Belt”, has been linked to a region of increased seasonal abundance of coccolithophores (Balch et al., 2011; Balch et al., 2016). Comparisons of in situ and remote sensing measurements of PIC have been undertaken in the Atlantic and Indian sectors of the SO for coccolithophore bloom conditions (e.g. Balch et al., 2014; Balch et al., 2016; Poulton et al., 2011). Nonetheless, this type of comparison is very limited in specific areas of the globe (such as the vast Pacific sector of the SO) but also in non-bloom coccolithophore conditions. This is partially due to the fact that available coccolithophore measurements are sparse in space and time in the SO. Many of the subpolar studies focus on coccospheres, whilst there are scarce data on free coccoliths (Mohan et al., 2008).

Changes in the calcification of *E. huxleyi* coccoliths have been shown in sub-Antarctic waters, with different morphotypes representing the genotypic response to different water chemistry (Cubillos et al., 2007). Other studies (e.g. Beaufort et al., 2011; Horigome et al., 2014; Young et al., 2014) point to an environmental control on different calcification levels of *E. huxleyi*. Several estimates of coccolith-PIC exist; e.g. estimation of coccolith-mass from coccolith volume calculated from coccolith-size (Young and Ziveri, 2000; Beuvier et al., 2019) or estimation of coccolith-calcite mass through calibration of its

birefringence signal at the light microscope (Beaufort, 2005; Bollmann, 2014; Fuertes et al., 2014). Comparisons between coccolith-estimated PIC and sea surface water scattering in the SO have targeted areas of coccolithophore blooms (Holligan et al., 2010; Poulton et al., 2011; Balch et al., 2014; Oliver et al., 2023), but so far this has only occasionally been done for non-bloom areas (e.g. Oliver et al., 2023).

Here, we focus on the contribution of *E. huxleyi* and other coccolithophore taxa to sea surface PIC along two latitudinal transects across the ACC fronts: a New Zealand transect (December 2004-January 2005) and a Drake Passage transect (February-March 2016). Coccosphere concentrations in the New Zealand transect were below  $1.4 \times 10^5$  cells/L and in the Drake Passage transect were below  $1.5 \times 10^5$  cells/L, corresponding to non-bloom to outer bloom conditions (Poulton et al., 2011). Our aims are: (1) to estimate the contribution of different coccolithophore taxa and morphotypes to PIC and (2) to compare coccolith-based PIC estimates with satellite-derived PIC values in the Pacific SO.

## **2 Study area: oceanographic setting and phytoplanktonic communities**

The SO is a high-nutrient, low-chlorophyll area in the Southern Hemisphere (e.g. De Baar et al., 1995) that connects all the main oceans through the strong and eastward flowing ACC. In the SO, there are a number of oceanographic fronts characterized by increased horizontal transport and rapid changes in water properties (Orsi et al., 1995; Klinck and Nowlin, 2001). The ACC is bounded by the Subtropical Front (STF) in the north, which separates it from the warmer and saltier waters of the subtropics, and its southern edge is marked by the Southern Boundary, which separates it from subpolar cold, silicate-rich waters (Orsi et al., 1995). Although the ACC flow is mostly driven by the westerly winds, the position of the fronts varies spatially and seasonally and it is also controlled by steep topographic features, such as oceanic plateaus or ridges (Gordon et al., 1978). South of the STF, the Subantarctic Front (SAF) separates the Subantarctic Zone (SAZ) and the Polar Frontal Zone (PFZ) (Fig. 1). The location of the SAF is indicated by a strong thermal gradient and by the rapid descent of a salinity minimum associated with the Antarctic Intermediate Water, from the surface in the PFZ ( $S < 34$ ) to depths greater than 300 m in the SAZ ( $S < 34.20$ ) (Orsi et al., 1995; Whitworth, 1980). South of the SAF, the prominent Polar Front (PF) separates the PFZ and the Antarctic Zone (AZ). The PF represents the northernmost extent of the  $2^\circ\text{C}$  isotherm at 200 m depth and corresponds to a  $2^\circ\text{C}$  gradient in sea surface temperature (Orsi et al., 1995). The Southern ACC Front is characterized by temperatures below  $0^\circ\text{C}$  at the minimum temperature in the sub-surface ( $< 150$  m) and above  $1.8^\circ\text{C}$  at the maximum temperature at depths  $> 500$  m (Orsi et al., 1995). A more detailed description of the property indicators at each SO front can be found in Orsi et al. (1995).

Coccolithophores dominate the SO phytoplankton communities, especially in the SAZ, where they reach relatively high numbers and diversity (e.g. Gravalosa et al., 2008; Saavedra-Pellitero et al., 2014; Malinverno et al., 2015; Charalampopoulou et al., 2016; Saavedra-Pellitero et al., 2019; Rigual Hernández et al., 2020a). On the other hand, diatoms and other siliceous microfossils dominate south of the PF (e.g. Saavedra-Pellitero et al., 2014; Malinverno et al., 2016; Cárdenas et al., 2018). The

coccolithophore abundance and diversity in the Drake Passage drastically drop from north to south, with the oceanographic fronts appearing to act as ecological boundaries (Saavedra-Pellitero et al., 2019), whereas the total coccolithophore abundance is highest in the PFZ south of New Zealand (Malinverno et al., 2015). Similar marked shifts at the SAF and PF in coccolithophore number, community composition, and diversity occurring were also previously noted in other sectors of the SO (e.g. Mohan et al., 2008; Gravalosa et al., 2008; Holligan et al., 2010; Saavedra-Pellitero et al., 2014; Balch et al., 2016; Charalampopoulou et al., 2016) and are in accordance with previous observations in both transects (Malinverno et al., 2015; Saavedra-Pellitero et al., 2019). In particular, the PF (Drake Passage) and the Southern ACC Front (New Zealand transect) constitute natural sharp barriers marked by a clear drop in the number of *E. huxleyi*, which often is the only species found in the PFZ and almost always occurs as B morphogroup (types B/C and O). Furthermore, a general southwards decreasing trend in *E. huxleyi* mass, linked to a latitudinal trend from more calcified *E. huxleyi* (A morphogroup) to weakly calcified morphotypes (B morphogroup), was already recorded across the Drake Passage (Saavedra-Pellitero et al., 2019).

### 3 Materials and methods

#### 3.1 Sampling considerations and morphometrics

##### 3.1.1 The New Zealand transect

Forty-two surface water samples were collected from the ship's pump of the *R/V Italica* (at ca. 3 m water depth) from 46.81°S to 69.37°S during the XX Italian Expedition from New Zealand to Antarctica from 31st December 2004 to 6th January 2005, (Fig. 1, Table 1). Details on sample locations, sampling volume, coccolithophore and coccolith counts can be found in Malinverno et al. (2015).

We selected a total of 13 water samples for Scanning Electron Microscope (SEM, Vega Tescan at the University of Milano-Bicocca) morphometric analyses of *E. huxleyi* covering the various biogeographic zones across the ACC (Fig. 1). For each sample, 30-50 images of *E. huxleyi* free coccoliths and coccospheres were collected as encountered during filter scanning (377 images in total, Table 1S in Supplementary Material). Distal shield length and width, tube thickness, and number and thickness of distal shield elements were manually measured using the ImageJ software (Schneider et al., 2012) in micrometers (μm) using the scalebar of the SEM images (Fig. 2).

##### 3.1.2 The Drake Passage transect

Nineteen water samples were collected on a transect at the western end of the Drake Passage (55.44°S to 61.75°S) during the *Polarstern* Expedition PS97 from 24th February 2016 to 5th March 2016 (Fig. 1, Table 1). These selected plankton samples were obtained using a rosette sampler with 24×12 L Niskin bottles (Ocean Test Equipment Inc.) attached to a CTD Seabird

159 SBE911plus device (Lamy, 2016). The bottles were fired by a SBE32 carousel and just the shallowest samples, from 5, 10 and  
160 20 m water depth, were considered in this work. Details on sample locations, sampling volume, coccolithophore assemblages  
161 and coccospheres/L can be found in Saavedra-Pellitero et al. (2019).

162

163 A total of 203 images of *E. huxleyi* coccospheres were taken from the samples in the Drake Passage while scanning the filters  
164 within another SEM (Zeiss DSM 940A at the Geosciences Faculty, University of Bremen; Table 2S in Supplementary  
165 Material). Coccoliths were measured using the Coccobiom2 macro (Young, 2015) in the software program Fiji, an image  
166 processing package based on ImageJ (Schindelin et al., 2012). Measurements were made in  $\mu\text{m}$ , based on the scale bar of the  
167 SEM images. Note that they were scaled to 100% with a Coccobiom2 SEM calibration of 1.09 and the specific magnification.

### 168 3.2 Coccolithophore PIC estimates

169 Species-specific coccolith-PIC (in pmol) was estimated following the volume calculation of Young and Ziveri (2000)

170

$$171 \text{ PIC} = (2.7 \times Ks \times L^3) \div 100 \quad [\text{equation 1}]$$

172

173 where:

174 2.7 = density of calcite;

175  $Ks$  = species-specific shape factors, as provided by Young and Ziveri (2000) and modified for *E. huxleyi* according to the  
176 degree of calcification obtained for each morphotype as compiled by Vollmar et al. (2022) (further details in Table 2);

177  $L$  = coccolith mean length from measurements in the case of *E. huxleyi*. For minor species, we considered the averaged  
178 coccolith length provided by Young and Ziveri (2000);

179 100 = molecular weight of calcite.

180

181 Measurements of the distal shield diameters of *Calcidiscus leptoporus*, the second most abundant species that is significantly  
182 larger and much more massive than *E. huxleyi*, were made on different samples offshore of New Zealand, corresponding to  
183 the highest abundances of this taxa (Table 2 and Table 3S in Supplementary Material). The importance of own size  
184 measurements for the determination of species-dependent coccolith PIC has been clearly emphasized (Baumann, 2004). The  
185 coccolith-PIC contribution for each sample was calculated by applying the obtained species-specific calcite quota to the  
186 abundances of species and morphotype (i.e., coccospheres/L) from Malinverno et al. (2015) and Saavedra-Pellitero et al.  
187 (2019) (Tables 1 and 2). In the New Zealand transect, the single / double coccolith layers were considered in the estimates  
188 (Table 1S in Supplementary Material), while in the Drake Passage transect, where this information was not available, an  
189 average was considered based on our own observations (Table 2 and Table 4S in Supplementary Material). Additionally,  
190 detached coccoliths/L were considered for the PIC estimates in the New Zealand transect (Malinverno et al., 2015). To estimate

the number of coccoliths per coccosphere we counted the visible placoliths (half coccosphere) and multiplied by two (e.g. Table 4S). We also calculated the relative tube width in *E. huxleyi* as a size-independent index to estimate the degree of calcification in this taxa following Young et al. (2014) (Fig. 2):

$$\text{Relative tube width} = (2 \times \text{tube width}) \div \text{coccolith width} \quad [\text{equation 2}]$$

Note that because the relative tube width is a ratio, it is dimensionless and it should be size-independent (Young et al., 2014).

### 3.3 Coccolith-estimated PIC errors

There are sources of errors and uncertainties linked to the approach chosen to estimate the coccolith PIC. To assess the reproducibility of the measurements, two different coccoliths were measured 50 times each. The standard deviation (SD) for the coccolith length was 0.014 and 0.017  $\mu\text{m}$  and the standard error 0.002  $\mu\text{m}$  in both cases. Coccolith volume estimates are likely to contain errors around 40-50% according to Young and Ziveri (2000), so we assumed the largest potential error and added a 50% error bars to our plots, although we note that measuring the actual size range in the sample can reduce this error to about 5-10% in length and 15-30% in volume.

### 3.4 Satellite-derived PIC and chlorophyll a data processing

To compare the coccolith-estimated PIC with satellite-derived values, PIC concentration in  $\text{mol m}^{-3}$  was obtained from the MODIS-Aqua Level (L) 2 and L3 products (NASA Goddard Space Flight Center, Ocean Ecology Laboratory, Ocean Biology Processing Group, 2022a). To encompass the broad range of PIC concentrations observed in the global ocean, a combination of two independent approaches is used to calculate the backscattering coefficient for PIC (the description of the algorithm can be found in NASA Ocean Biology Processing Group, 2023; for further details see also Balch and Mitchel, 2023). The Ocean Biology Processing Group (OBPG) validates MODIS-Aqua PIC retrievals against in situ measurements, which results in a mean bias of  $\pm 0.31623$  and a mean absolute error (MAE) of  $\pm 3.91664$  (both values calculated based on log10 transformation to the PIC values) (<https://oceancolor.gsfc.nasa.gov/data/reprocessing/r2022/aqua/>). These metrics indicate the degree of accuracy and potential bias in the satellite-derived estimates compared to direct observations.

MODIS-Aqua L2 scenes encompassing both the sampling period and the geographical extent of each transect were downloaded from NASA's Ocean Colour L1 and L2 browser (<https://oceancolor.gsfc.nasa.gov/cgi/browse.pl>). The downloaded MODIS L2 scenes corresponded to swaths covering at least 50% of the study area and included more than one

daily scene. Table 3 summarizes the number of downloaded scenes as well as their time coverage. To obtain satellite-derived PIC concentrations for comparison with coccolith-estimated PIC at each sample location, the mean of a 5x5 window centered on the measurement location (Bailey and Werdell, 2006) was extracted from the downloaded scenes using the SNAP 9.0.0 pixel extraction tool (European Space Agency (ESA), 2022). This tool provides basic statistics, such as the number of pixels (N) contributing to each mean value and the SD of these pixel values, allowing the homogeneity of the extraction point to be assessed. Pixels flagged with atmospheric correction failure (ATMFAIL) or very low water-leaving radiance (LOWLW) were excluded from the extraction. To ensure statistical confidence in the retrieved values, all PIC mean values resulting from the aggregation of 12 or fewer N within the 5x5 window were discarded (Bailey and Werdell, 2006). Duplicate daily mean PIC values (i.e. PIC values for a measuring location extracted from more than one scene captured on the same day) and their corresponding SD were then weighted according to their uncertainties (Bevington, 1969) to give more prominence to measurements with a lower SD, which are generally considered to be more reliable. However, daily mean values with SD equal to zero were used directly as the result, since the value with zero SD suggests homogeneity.

Due to high cloud cover and other conditions that interfere with the detection of water-leaving radiances (NASA Ocean Biology Processing Group, 2023), daily PIC grids yielded a high number of missed observations, or gaps, which prevented us from acquiring daily satellite-derived PIC values of the sampling dates for most sample locations in both transects (Figs. 1S and 2S in Supplementary Material show the availability of MODIS-Aqua L2 PIC values across stations over the sampling period). This data scarcity made it impossible to use a time window of 24 h to determine coincidence between coccolith-estimated PIC and satellite-derived PIC. Therefore, to increase data availability, we (1) extended the satellite period to seven days before and after sampling dates (see Table 3 for specific dates) and extracted the PIC for all sample locations, regardless of their sampling date. We deliberately chose that time range considering that *E. huxleyi* can double its numbers in two or three days without accounting for grazing by zooplankton (based on studies in the North Atlantic; Holligan et al., 1993), ensuring no drastic changes from non-coccolithophore bloom to bloom conditions. We then generated a mean PIC value for each location by aggregating the available daily means over the full period to explore the latitudinal variation of this variable; and (2) also obtained monthly (Figs. 3S and 4S in Supplementary Material) and 8-daily (going forward, referred to as weekly) satellite-derived PIC concentrations ( $\text{mol m}^{-3}$ ) from the MODIS-Aqua L-3 product (NASA Goddard Space Flight Center, Ocean Ecology Laboratory, Ocean Biology Processing Group, 2022b). This allowed us to have additional satellite-derived PIC values to compare to the coccolith-estimated PIC in the study area. Images encompassing both the sampling period and the geographical extent of each transect, were acquired from NASA's Ocean Color Level 3 and 4 Browser (<https://oceancolor.gsfc.nasa.gov/l3/>) as 4 km cell size gridded files in NetCDF file format. Table 3 summarizes the number of downloaded scenes as well as their time coverage. The L3 extracted values corresponded to the PIC concentration of the grid cell enclosing the sample location. As per L2 data extraction, PIC concentrations for all sample locations were acquired from all available monthly and weekly scenes. MODIS-Aqua L2 chlorophyll a concentration in  $\text{mg m}^{-3}$  were also extracted



255 and processed as an indicator of the presence of diatoms and other phytoplanktonic groups. The algorithm used to calculate  
256 chlorophyll a is documented by Werdell et al. (2023).

## 257 **4 Results**

### 258 **4.1 Coccolith-estimated PIC versus satellite-derived PIC**

259 *Emiliania huxleyi* is the dominant species in the coccolithophore assemblage of the Pacific SO (Malinverno et al., 2015;  
260 Saavedra-Pellitero et al., 2019) with abundances of  $1.4 \times 10^5$  coccospheres/L (at station TR033) south of the SAF in the New  
261 Zealand transect and  $1.5 \times 10^5$  coccospheres/L (at station PS97/034-2) in the Drake Passage SAZ and it is also the main  
262 contributor to sea-surface PIC (Figs. 3 and 4). *Calcidiscus leptoporus* (mostly the intermediate-sized form) is the second most  
263 abundant species and makes significant contributions to the coccolithophore PIC at certain locations (up to  $1.4 \times 10^4$  cells/L in  
264 the New Zealand transect and  $1.4 \times 10^3$  cells/L in the Drake Passage, Figs. 3 and 4) (Malinverno et al., 2015; Saavedra-Pellitero  
265 et al., 2019). *Calcidiscus leptoporus* generally represents on average 20.2% of the total coccolithophore PIC in the New  
266 Zealand transect and 5.3% in the Drake Passage, but can occasionally reach maximum PIC contributions of 68.3% (at station  
267 TR008, in the SAZ) and of 31.1% (at station PS97/017-1, in the SAZ) (Fig. 5).

268  
269 A minor contribution from less abundant or rare species is found in the northern SAZ of both transects, where diversity is  
270 higher (for species list see Malinverno et al., 2015; Saavedra-Pellitero et al., 2019), with a poleward decreasing trend and  
271 almost no contribution south of the SAF (Fig. 5). *Emiliania huxleyi* is responsible for almost all of the coccolith-estimated PIC  
272 in the PFZ, but its contribution decreases at the PF (in the Drake Passage) and Southern ACC Front (in the New Zealand  
273 transect, ca. 63.7°S) and further south. Daily, weekly and monthly satellite (MODIS-Aqua L2)-derived PIC at the sampling  
274 locations are generally higher than coccolith-estimated PIC in both transects; this difference is larger in the Drake Passage  
275 (Fig. 4) than in the New Zealand transect (Fig. 3). There are discrepancies in absolute values (on top of the already inherent  
276 variations in the weekly compared to the monthly PIC estimates and the limited availability of L2 data). These are particularly  
277 obvious at the PF (ca. 60°S in the Drake Passage) or to the south of it (ca. 62.5°S in the New Zealand transect), where the  
278 satellite-derived and coccolith-estimated PIC become decoupled, characterized by high reflectance but no coccolithophores in  
279 the AZ.

### 281 **4.2 Morphometries and mass estimates of *Emiliania huxleyi***

282 *Emiliania huxleyi* consist of different morphotypes that show a different and partly overlapping distribution along both  
283 latitudinal transects (Malinverno et al., 2015; Saavedra-Pellitero et al., 2019). Type A is mostly restricted to the northern SAZ,  
284 but it is occasionally present in the PFZ in the Drake Passage (Figs. 3, 4) and it is the only type within morphogroup A in this  
285 study. Morphotypes belonging to the *E. huxleyi* morphogroup B (which includes morphotypes B, B/C, C and O) are present in

the SAZ and the PFZ, but they disappear south of the PF. Morphometric measurements on coccoliths of *E. huxleyi* from the selected samples show that the length of types A, B/C-C and O overlap in both transects (Fig. 6). In the Drake Passage, coccolith lengths range from 2.86 to  $3.96 \pm 0.43 \mu\text{m}$  (unless specified,  $\pm$  refers to the SD from now on) with a mean average of  $3.49 \pm 0.33 \mu\text{m}$  for A type (including normal and overcalcified specimens), 2.87 to  $4.11 \pm 0.45 \mu\text{m}$  for B type, 2.20 to  $3.98 \pm 0.37 \mu\text{m}$  for B/C-C types, 2.42 to  $4.16 \pm 0.41 \mu\text{m}$  for O type, and an average of  $2.98 \pm 0.40 \mu\text{m}$  for morphogroup B. In the New Zealand transect, maximum lengths range from 2.25 to 3.59  $\mu\text{m}$ , with an average of  $2.95 \pm 0.28 \mu\text{m}$  for *E. huxleyi* type A, 1.95 to  $3.62 \pm 0.33 \mu\text{m}$  for B/C-C types, 2.07 to  $4.14 \pm 0.36 \mu\text{m}$  for type O, and an average of  $2.87 \pm 0.35 \mu\text{m}$  for morphogroup B.

Figure 6 provides a latitudinal overview of morphometric data compared to the (averaged) degree of calcification (indicated by the dimensionless relative tube width index; Young et al., 2014). In the New Zealand transect there are no significant changes in coccolith lengths except for a wide scatter of values characterizing the size class distribution of each sample. This feature reflects the large variability in coccolith size as observed on coccoliths from a single coccosphere (Fig. 2e). However, in the Drake Passage transect, *E. huxleyi* coccoliths are notably larger offshore of Chile (Fig. 6a).

*Emiliania huxleyi* masses calculated in the New Zealand transect range from 0.61 to 2.93 pg with an average of  $1.47 \pm 0.46$  pg per coccolith belonging to the morphogroup A, and from 0.36 to 2.86 pg, with an average of  $1.15 \pm 0.43$  pg per coccolith from morphogroup B (Fig. 3e). In the Drake Passage the masses per coccolith for morphogroup A are almost double than in the New Zealand transect, varying between 1.39 pg and 6.26 pg, with an average of  $3.00 \pm 1.19$  pg. The coccolith masses in morphogroup B range from 0.57 to 3.75 pg with a mean of  $1.44 \pm 0.62$  pg across the Drake Passage (Fig. 4e). The coccolith-estimated PICs for just the species *E. huxleyi* are generally lower in the New Zealand transect (average morphogroup A:  $0.021 \pm 0.010$  pmol and B:  $0.013 \pm 0.006$  pmol, considering 50% potential error) than in the Drake Passage (average morphogroup A:  $0.034 \pm 0.017$  pmol and B:  $0.014 \pm 0.007$  pmol -error-).

We observed that some coccoliths are clearly overcalcified (see Fig. 6), with a thick inner tube (up to 0.76  $\mu\text{m}$  in sample PS97/018-1) that extends into the central area. Specimens belonging to the morphogroup A show a higher degree of calcification than those belonging to morphogroup B, resulting not only in a thicker inner tube but also in thicker distal shield T-elements. The overcalcified coccospheres co-occur with normally-calcified ones but they are restricted to the northernmost samples (Fig. 6). The relative tube width (as an index for calcification), calculated using equation 2, varies from 0.10 to  $0.28 \pm 0.04$  in morphogroup A and from 0.07 to  $0.21 \pm 0.03$  in B for the New Zealand transect. Values are higher in the Drake Passage, ranging from 0.05 to  $0.50 \pm 0.12$  for *E. huxleyi* morphogroup A, and from 0.02 to  $0.22 \pm 0.04$  for morphogroup B. The degree of calcification is highly variable within each sample of the New Zealand transect (Fig. 3d), but overcalcified specimens (relative tube width  $>0.23$ ), typically represented by type A, only occur in the northernmost samples (Fig. 6b). The averaged relative tube width index shows increased values not only in the SAZ offshore of New Zealand, but also around 54°S

and in the PFZ (Figs. 3d, 6b), which points to a certain degree of variation in the calcification within morphotypes BC/C and O. A more marked N-S decrease in the relative tube width index values is observed in the Drake Passage, with notably higher values offshore of Chile (Figs. 4d and 6a), where relatively large and heavily calcified type A coccospheres are present.

## 5. Discussion

### 5.1 PIC variability in the SAZ and PFZ

In the studied transects, even with the limited data available, the coccolith-estimated PIC and the satellite-derived PIC show a comparable trend in the SAZ and PFZ, but there is a strong discrepancy in the AZ (Fig. 5S in the Supplementary Material). The fact that satellite-derived PIC is generally higher than coccolith-estimated PIC in the SAZ and PFZ (Figs. 3, 4 and 5S in the Supplementary Material) could be due to an underestimation of the species specific coccolith-estimated PIC. The potential assumptions linked to the coccolith-estimated PIC, including shape factors (Ks), average coccolith length (L), number of coccoliths per coccosphere, and/or number of coccolith layers per cell (Table 2), have associated uncertainties. Even if we tried to minimize these by measuring the actual coccolith size range and counting coccoliths per coccosphere (instead of using assumed values), the overall error can still add up to  $\pm 50\%$  (Young and Ziveri, 2000). Additionally, the fact that the difference between satellite-derived PIC and coccolith-estimated PIC in the Drake Passage transect is larger than in the New Zealand transect can be also in part attributed to the fact that detached coccoliths (in addition to coccospheres) were only considered in the estimates for the New Zealand transect.

Given that *E. huxleyi* is the dominant species and the main contributor to coccolith-estimated PIC in the SAZ and PFZ of both transects (Fig. 5), we focused on its abundance, morphotype distribution and calcite weight to assess potential PIC discrepancies. Coccolith-estimated PIC for *E. huxleyi* are generally in agreement with the calcite content per coccolith obtained by Poulton et al. (2011) along the Patagonian Shelf and by Rigual Hernández et al. (2020a) in the Australian and New Zealand sectors of the SO (see Tables 1 in those papers). Our *E. huxleyi* PIC estimates seem generally higher than the estimates by Charalampopoulou et al. (2016) off southern Chile (0.015 pmol per coccolith) and across the rest of Drake Passage ( $< 0.009$  pmol). On the other hand, our values are slightly lower than those obtained through the birefringence method SYRACO, an automated system of coccolith recognition (SYstème de Reconnaissance Automatique de COccolithes) in the same latitudinal range (e.g. Beaufort et al., 2011), and notably lower than Saavedra-Pellitero et al. (2019), who used circularly polarized light plus the C-Calcita software developed by Fuertes et al. (2014) across the Drake Passage (Fig. 7a). In order to explore this difference, we calculated PIC in the Drake Passage using the Saavedra-Pellitero et al. (2019) mass estimates for the same samples, considering an average mass of  $4.64 \pm 2.53$  pmol for *E. huxleyi* ( $n = 796$ ), but without distinguishing different morphotypes (Fig. 7c). The mass per coccolith of *E. huxleyi* using C-Calcita in the Drake Passage is 2.8 times higher than in this study (mean of  $1.66 \pm 0.91$  pg here). We then extrapolated the potential contribution of the rest of the coccolithophore

352 taxa using this factor (i.e., multiplying by 2.8 the *C. leptoporus* and minor species PIC values calculated in this study) (Fig.  
353 7c). Both N-S coccolith mass and PIC trends mirror each other, but the C-*Calcita*-derived PICs tend to overestimate satellite-  
354 derived PIC values, except in a couple of locations. This can be attributed to the calibration of the coccolith thickness within  
355 the software C-*Calcita*, which has been improved in recent years with the use of a calcite wedge instead of a calcareous spine  
356 (e.g. Guitián et al., 2022).

357  
358 The generally higher satellite-derived PIC numbers compared to the coccolith-estimated PIC values in the SAZ and PFZ (Figs.  
359 3, 4, and 5S in Supplementary Material) could be also due to the presence of other carbonate-forming organisms (and/or their  
360 fragments); for instance, foraminifera, can contribute to a significant fraction of the total PIC in the SO south of Australia,  
361 especially between 55-60°S (Trull et al., 2018). We do not have data for the Drake Passage, but planktonic foraminifera were  
362 observed in the filter samples across the New Zealand transect, showing increased abundance (together with the tintinnid  
363 species *Codonellopsis pusilla*) in the PFZ (see Malinverno et al., 2016 for further details). Although foraminifera and other  
364 hard-shelled micro-zooplankton PIC particles provide negligible backscatter per unit mass (Balch et al., 1996), they can be a  
365 source of error in the PIC volume calculation when considering only coccolithophores. Assessing the significance of carbonate-  
366 forming organisms relative to other taxa in the SO is an important topic, but falls beyond the scope of this paper.

367  
368 Observed discrepancies between satellite-derived PIC and coccolith-estimated PIC values can arise from a combination of  
369 several factors related to the PIC algorithm sensitivities and limitations (Mitchell et al., 2017; Balch and Mitchell, 2023; NASA  
370 Ocean Biology Processing Group, 2023), differences in spatial and temporal resolution (Table 3), and environmental factors  
371 (e.g. turbidity or other particulate matter that can affect the accuracy of satellite-derived PIC estimates). MODIS-derived L2  
372 PIC data was limited due to the cloudy skies of the SO during the sampling period (see Figs. 1S and 2S in the Supplementary  
373 Material). To mitigate the impact of these data gaps in our analysis, we extended the time window for data extraction to several  
374 days and computed the mean for each location, whilst also using L3 products. This approach, while necessary, could obscure  
375 potential variability at shorter temporal scales and create discrepancies when comparing with sample measurements taken on  
376 specific days. The fact that the overall trends are comparable in the New Zealand and Drake Passage transects (Fig. 5S in the  
377 Supplementary Material), could also suggest a satellite bias linked to the algorithm. We are aware that the MODIS-Aqua  
378 Ocean Color was re-processed in 2022 to incorporate updates in instrument calibration, new ancillary sources and algorithm  
379 improvements (NASA Ocean Biology Processing Group, 2023a), but the validation of the PIC measurements was based on a  
380 low number of in-situ measurements compared to other products (e.g. 1347 in situ measurements for chlorophyll a and just 42  
381 for PIC, all of them in the Atlantic Ocean; NASA Ocean Biology Processing Group 2023b). The differences in PIC could also  
382 be due to the fact that we are comparing in situ values to weekly and monthly averages, as well as also smoothing data by  
383 considering averaged values when estimating coccolith-estimated PIC (especially length and number of coccoliths per  
384 coccosphere). In addition, sampling at slightly different times of the year may also have an influence on the PIC values  
385 determined (Rigual Hernández et al., 2018; Rigual-Hernández et al., 2020a, b).

386 In general, we find a different pattern to that described in Balch et al. (2014), who determined coccolith-quotas in the center  
387 of a coccolithophore bloom in the Patagonian Shelf (Atlantic Ocean) ranging from 0.008 to 0.017 pg per coccolith by  
388 comparing automated coccolith-counts with coccolith-estimated PIC. In the context of other observations, the coccolith quotas  
389 calculated by Balch et al. (2014) are relatively low and show a much greater variation within a limited region. Considering the  
390 differences in the two SO transects studied here, which were sampled 11 years apart, we could assume that with our approach,  
391 the surface coccolith-estimated PIC (up to 20 m water depth) underestimate satellite-derived PIC concentrations in the SAZ  
392 and PFZ. This discrepancy is evident in our data, where coccolith-estimated PIC concentrations calculated using different  
393 methodologies, such as C-Calcita, exceed those obtained from the satellite data. This indicates that there is still a need for  
394 improved precision in coccolith-estimated PIC concentration methods. Therefore, it is crucial to refine existing methods and  
395 develop new algorithms to enhance accuracy. Additionally, the limited number of in situ data points used for calibrating  
396 satellite algorithms in the SO could contribute to these discrepancies, highlighting the importance of expanding in situ datasets  
397 for better validation and calibration of remote sensing data.

## 398 **5.2 Assessing potential biases in PIC estimates for the AZ**

399 In the AZ (south of about 62.5°S in the New Zealand transect and about 60°S in the Drake Passage), high reflectance is detected  
400 by remote sensing but is not associated with a coccolithophore bloom (Figs. 3, 4 and S5). Concentrations of *E. huxleyi*, which  
401 show maximum numbers in the PFZ at the New Zealand transect and moderate values in the Drake Passage, drop southward  
402 of this location at the Southern ACC Front and the PF (Malinverno et al., 2016). Satellite data show the different impact of  
403 ACC fronts on the distribution of *E. huxleyi* (Holligan et al., 2010): in the Drake Passage, where the fronts are strictly  
404 constrained by topography, *E. huxleyi* is bounded by the PF to the south (Saavedra-Pellitero et al., 2019), while in the eastern  
405 Scotia Sea, where the ACC fronts are broadly separated, *E. huxleyi* spreads between the PF and the Southern ACC Front  
406 (Holligan et al., 2010; Poulton et al., 2011; Poulton et al., 2013). This pattern also emerges from the compilation by Malinverno  
407 et al. (2016), which shows that the Southern ACC Front marks the southern boundary in different SO sectors.

408  
409 Occasional occurrences of *E. huxleyi* south of the Southern ACC Front have been documented south of Tasmania and in the  
410 Weddell sea in certain years by conventional micropalaeontological observations (e.g. Winter et al., 1999; Cubillos et al.,  
411 2007) as well as in the Australian sector of the SO and in the Scotia Sea using surface reflectance data only (Holligan et al.,  
412 2010; Winter et al., 2014). However, in our study, *E. huxleyi* is constrained by the Southern ACC Front corresponding to a  
413 maximum sea surface temperature of 1°C in the New Zealand transect.

414  
415 The magnitude and spectral characteristics of water-leaving radiance detected by satellites are influenced by the inherent  
416 properties of the optically active constituents. These include: (1) light scattering by PIC, other biogenic particles or lithogenic  
417 material (e.g. Bi et al., 2023) as well as (2) light absorption by phytoplankton biomass (i.e., chlorophyll a concentration) and  
418 dissolved organic matter (e.g. Reynolds et al., 2001; Ferreira et al., 2009). The strong correlation between high values of water-

leaving radiance and high *E. huxleyi* PIC concentrations has been successfully proved in bloom areas (e.g. Gordon et al., 1988; Balch et al., 2005; Holligan et al., 2010; Balch et al., 2011; Balch et al., 2014; Balch and Mitchell, 2023; Oliver et al., 2023). However, not all bright waters are caused by *E. huxleyi* blooms, as shown by Broerse et al. (2003) in the Bering Sea, Balch et al. (2007) in the Gulf of Maine, and Daniels et al. (2012) in the Bay of Biscay. Suspended particles, which include either reworked coccoliths, lithogenic material or empty diatom frustules, could be responsible for high values of water-leaving radiance, at least in nearshore regions (Broerse et al., 2003; Balch and Mitchell, 2023).

The occurrence of bright waters along the studied transects should theoretically be constrained by the position of the PF/Southern ACC Front. Malinverno et al. (2015; 2016) showed a significant shift in the community composition from carbonate to silica-dominated microfossils in the New Zealand transect at the Southern ACC Front, with diatoms being the most abundant mineralized phytoplankton group in the transect (Fig. 3k). Coccolithophores disappear south of the Southern ACC Front, and the composition of the siliceous phytoplankton changes from a dominance of large diatoms (*Fragilariopsis kerguelensis*) in the north to a dominance of small diatoms (such as the cold adapted *Fragilariopsis cylindrus*) in the south, with a notable increase in spiny silicoflagellates (e.g. *Stephanocha speculum* var. *coronata*) and small siliceous plankton (Parmales, Archaeomonads) (Malinverno et al., 2016) coincident with high values of chlorophyll a in the AZ (Figs. 3l, 8). Extant diatoms have not yet been studied in the exact same water samples collected during PS97 Expedition. However, the abundance of subfossil diatoms in surface sediments in the Drake Passage shows an increase south of the PF, along with an increase in the relative abundance of siliciclastics, biogenic opal (Cárdenas et al., 2018). This contrasts with the relatively low satellite-derived chlorophyll a concentration in the AZ (Fig. 4k), but this only due to the very limited number of daily L2 data available. *Fragilariopsis kerguelensis* appears to dominate up to the Southern ACC Front, and *F. cylindrus* is found south of this front, in colder waters of the Drake Passage (Cárdenas et al., 2018).

Different alternatives have been suggested for the high reflectance in the AZ of the SO, such as microbubbles (mostly during storms), floating loose ice, high concentrations of other particulate matter such as glacial flour (especially close to the Antarctic continent) or *Phaeocystis* blooms (Balch et al., 2011; Balch, 2018; Balch and Mitchell, 2023). Our observations do not allow us to comprehensively determine the potential causes of this high reflectance, but we note that a high abundance of small opal biogenic particles, such as small-size diatoms, silicoflagellates and siliceous plankton observed (as well as their fragments) would be consistent with the observed high scattering of these waters at least in the New Zealand transect (Figs. 1, 3, 4, 3S and 4S in Supplementary Material), even though opal particles have a much lower refractive index than calcite (Balch, 2009; Costello et al., 1995).

### 5.3 *Emiliana huxleyi* morphotypes

*Emiliana huxleyi* morphometric dataset reveals that type A overcalcified morphotype is highly distinct from the other morphotypes (Fig. 6). This morphotype has also been previously observed in the coastal waters of the eastern South Pacific

and in the open ocean (Beaufort et al., 2011; Von Dassow et al., 2018; Saavedra-Pellitero et al., 2019). However, it should be noted that type A overcalcified in this work includes the moderately calcified, robustly calcified and extremely heavily calcified A morphotypes described by Diaz-Rosas et al. (2021). Coccospheres of *E. huxleyi* classified by Diaz-Rosas et al. (2021) as extremely heavily calcified R/hyper-calcified and/or A-CC morphotypes (with complete overgrowth of the coccolith central area but without fusion of distal shield elements) occasionally occurred offshore of Chile in samples closest to the coastline (see an example in Fig. 6). In the Southern Hemisphere, these extremely heavily calcified morphotypes were only previously observed at the Pacific border of southern Patagonia (in the Archipelago Madre de Dios Fjord area) and in the Northern Hemisphere, in Norwegian fjords (e.g. Young et al., 2014). Diaz-Rosas et al. (2021) suggested that the R/hyper-calcified morphotype has a marginal ecological niche preference compared to moderately calcified types A and A-CC. Therefore, the few specimens of *E. huxleyi* type A overcalcified (i.e. heavily calcified looking in between the R/hyper-calcified and/or A-CC morphotypes by Diaz-Rosas et al. (2021)) observed in this work, and by Saavedra-Pellitero et al. (2019) in the Drake Passage, could be attributed to different niches overlapping offshore of Chile.

The normal type A specimens show a moderate range of variation in tube width, comparable to type O, but smaller than B, B/C-C, with type C having the thinnest tube width. The distal shield element width and the number of T-elements of the different specimens are closely related to the length and width measured (Fig. 6) as they are all indicators of coccolith size. There is broader variation in coccolith size (length and width) within morphogroup B compared to morphogroup A, which is more restricted. Suchéras-Marx et al (2022) pointed out that *E. huxleyi* coccolith size is limited by the cell diameter because heterococcoliths are produced intracellularly and are extruded later on. Interestingly, specimens of *E. huxleyi* type A in the New Zealand transect are notably smaller than those offshore of Chile, which we link to local adaptations, seasonality and even ecological interactions such as predation (e.g. Monteiro et al., 2016; Hansen et al., 1996).

However, the coccolithophore assemblages in the PFZ and south of it are monospecific, which is also known from other areas of the SO (e.g. Charalampopoulou et al., 2016), and consist almost entirely of *E. huxleyi* morphogroup B. The mean placolith length of *E. huxleyi* morphogroup B (including types B, B/C-C, and O) in both transects is very similar (Drake Passage:  $2.98 \pm 0.40 \mu\text{m}$ , New Zealand:  $2.87 \pm 0.35 \mu\text{m}$ ) and agrees well with the corresponding B/C measurements of Charalampopoulou et al. (2016) in samples retrieved in 2009 in the Drake Passage ( $2.8 \mu\text{m}$ ). Still, our averaged values are slightly lower than the mean length estimated by Poulton et al. (2011) on the Patagonian Shelf ( $3.25 \pm 0.40 \mu\text{m}$ ). This could be due to the fact that Poulton et al. (2011) did not distinguish between types B and O (i.e. they were merged into B/C), which are typically larger coccoliths than B/C (Fig. 6) and could have contributed to increase the averaged length. The length range for types B/C-C (Drake Passage:  $2.20$  to  $3.98 \pm 0.37 \mu\text{m}$ , New Zealand:  $1.95$  to  $3.62 \pm 0.33 \mu\text{m}$ ) agrees quite well with the range reported by Cook et al. (2011) for cultured B/C strains ( $2.65$  to  $4.80 \mu\text{m}$ ) and is in the range of sizes presented by Charalampopoulou et al. (2016) for the Drake Passage ( $1.8$  to  $5.5 \mu\text{m}$ ). The fact that we record lower values is simply a matter of taxonomical considerations regarding the overlapping sizes of morphotypes B, B/C, C and O, visually represented in Figure 6.

487

488 Overall, our morphometric data from selected samples along the New Zealand and Drake Passage transects show (1)  
 489 differences in calcification between the different *E. huxleyi* morphotypes, which are particularly evident in type A (Figs. 3, 4,  
 490 5, and 6), (2) a large scatter of relative tube width within morphotypes and within each sample, particularly pronounced in the  
 491 New Zealand transect (Figs. 4, 6), and (3) a slight decreasing trend in coccolith size and degree of calcification in the Drake  
 492 Passage (Figs. 3, 6), which is not observed in the New Zealand transect. This suggests that environmental influences have no  
 493 significant effect on the degree of calcification, but clearly control the distribution of *E. huxleyi* morphotypes (which are  
 494 genetically-determined; Bendif et al., 2023) and thus indirectly affect the coccolith mass variation. This could also explain the  
 495 southwards decreasing trend in calcification in the Drake Passage, as the relatively large and heavily calcified type A  
 496 coccospheres occur in the northern SAZ

497

498 The different taxonomic considerations of *E. huxleyi* in different studies make it difficult to compare and combine data,  
 499 especially in light of recent advances in the field. Given the dominance of this taxa in the SO, a key area for global warming  
 500 and ocean acidification studies, efforts by the scientific nanofloral community should focus on a more uniform classification  
 501 of *E. huxleyi* morphotypes. However, differentiation and recognition of the various morphotypes is time consuming and tedious  
 502 and plays only a minor role in the calculation of the total coccolithophorid PIC, as observed in other areas of the SO (e.g.  
 503 Rigual Hernández et al., 2020a, b). The changes in mass within the B morphotype (with types B/C-C, C, O) in the two transects  
 504 are negligible in the PIC calculation, while a differentiation into morphogroups A and B has an influence on the calculation of  
 505 the PIC. However, specimens of *E. huxleyi* belonging to morphogroup A only occur in the northern areas of both transects,  
 506 where they play a role together with the PIC input from other massive species such as *C. leptoporus* (Fig. 5). Overall, the  
 507 changes in total coccolithophore-PIC in the study area are caused by the abundance and occurrence within the entire  
 508 coccolithophore community. The relative contribution of the different *E. huxleyi* morphogroups to the coccolithophore-PIC in  
 509 the SO deserves further exploration in light of the rapid development of remote sensing and recent evolution of machine  
 510 learning approaches for PIC estimates.

## 511 6 Conclusions

512 The comparison between particulate inorganic carbon (PIC) derived from satellite data and in situ coccolithophore-based  
 513 estimates in two transects of the Pacific sector (separated in time and space) demonstrates the limited availability of high-  
 514 quality satellite-derived data (mostly due to atmospheric conditions), and the need for refining methodologies to accurately  
 515 produce coccolith-estimated PIC. Based on our data the following conclusions can be drawn:

516

- 517 1) We found that satellite-derived PIC values and coccolith-estimated PIC values follow a comparable trend in the  
 518 Subantarctic Zone (SAZ) and Polar Front Zone (PFZ). However, satellite-derived PIC values are generally higher



than coccolith-estimated PIC. This difference could be due to a lack in precision in the coccolith-based PIC estimates, to the presence of foraminifera and/or other hard-shelled micro-zooplankton adding potential error when calculating total PIC volume, or to a certain bias in the algorithm due to the low number of measurements used for the validation of the satellite-derived PIC calibration (all of which were taken in the Atlantic Ocean).

- 2) There is an observed decoupling of satellite-derived PIC and coccolith-estimated PIC south of the Polar Front (PF), in the Antarctic Zone (AZ). Despite having satellite high reflectance values, no coccolithophores were observed in this area of high chlorophyll a concentration. We are unable to determine the reason for this with our data, but note that an abundance of small biogenic opal particles, such as small-size diatoms, silicoflagellates and/or siliceous plankton (as well as their fragments) or, potential biogenic particles not visible in scanning electron microscope (e.g. *Phaeocystis* aggregations, microbubbles, etc.) could possibly provide an explanation for this observation.
- 3) *Emiliania huxleyi* is the predominant coccolithophore species contributing the most to the total sea-surface coccolith-PIC in the New Zealand transect (mainly sampled in 2005) and as well as in the Drake Passage (sampled in 2016). *Calcidiscus leptoporus* may occasionally contribute significantly to the total coccolithophore-PIC at certain locations, whereas the rest of the coccolithophore taxa contribute only marginally in the studied areas.
- 4) *Emiliania huxleyi* consists of several morphotypes, which have different, partly overlapping geographical distributions. The relatively massive type A occurs in the northern SAZ and occasionally in the PFZ of the Drake Passage, while specimens of the less calcified morphogroup B (which includes types B, B/C, C and O) occur in the SAZ and the PFZ of both transects, but disappear drastically south of the PF. But neither the slightly different carbonate masses nor the southward changes in morphotype composition have a decisive influence on the coccolith-estimated PIC, which is only determined by the abundance of *E. huxleyi* in this area.

The satellite-derived and coccolith-estimated PIC discrepancies observed in this work emphasize the importance of in situ measurements and sampling; it also highlights the need for further investigation to fully understand the factors influencing water-leaving radiance and the reliability of remote sensing estimates, especially south of the PF. Future research should focus on refining methodologies and satellite algorithms to improve the accuracy of PIC estimates and better understand the dynamics of coccolithophores as well generally phytoplankton and zooplankton communities in the Pacific sector of the Southern Ocean (especially compared to other sectors). Such efforts will enhance our understanding of carbon cycling and its impact on marine ecosystems at high latitudes.

## 550 Acknowledgements

551 Stellite-derived Particulate Inorganic Carbon (PIC) data was downloaded from the Ocean Color Web Level 1 & 2 Browser  
552 (<https://oceancolor.gsfc.nasa.gov/cgi/browse.pl?sen>) and Level 3 & 4 Browser (<https://oceancolor.gsfc.nasa.gov/l3>), both of  
553 them services provided by NASA's Ocean Biology Distributed Active Archive Centre (OB.DAAC).

554 The authors acknowledge the use of the JASMIN (Joint Analysis System for the Met Office, NERC, and UKRI)  
555 (<https://jasmin.ac.uk/>) Jupyter Notebook service to process the satellite-derived PIC data. We would like to express our  
556 gratitude to the JASMIN team for their support and the valuable resources they provide to the scientific community.

557 The authors are grateful to two anonymous reviewers and to the handling associate editor, Prof. Shutler, for their invaluable  
558 suggestions on a previous version of the paper. The Alfred Wegener Institute Bremerhaven provided part of the plankton  
559 samples required for this study. Frank Lamy, Hartmut Schulz, *R/V Polarstern* officers and crew are thanked for their help  
560 during the PS97 Expedition.

561 Dr. Frigola (Barcelona Supercomputing Center, Spain), Dr. Merkel (University of Bremen/MARUM, Germany) and Dr.  
562 Hardiman (University of Portsmouth, UK) are acknowledged for their help with remote sensing data collection advice. Dr.  
563 Pepin (University of Portsmouth, UK) and Dr. Balch (Bigelow Laboratory for Ocean Sciences, USA) are thanked for their  
564 comments and suggestions on this piece of research during the "Advances in Coccolithophore research" meeting. Dr. Saavedra  
565 (RIP) is thanked for his continuous encouragement to finish up this paper.

## 566 Financial support

567 This research was supported by the University of Portsmouth, by the Deutsche Forschungsgemeinschaft with a grant to Karl-  
568 Heinz Baumann (reference number: BA 1648/30-1) -through previous funding for Mariem Saavedra-Pellitero and Nele M.  
569 Vollmar- and by the MIUR project "Dipartimenti di Eccellenza 2018/2023" for Elisa Malinverno, at the Department of Earth  
570 and Environmental Sciences, University of Milano-Bicocca. The University of Portsmouth Research and Innovation Services,  
571 as well as Copernicus Publications are acknowledged for their additional financial support to publish this paper as Open  
572 Access.

## 574 Data Availability Statement

575 The authors confirm that the data from which the findings of this study are available within the article Supplementary Materials  
576 and are stored in the data repository <https://pangaea.de/> (<https://doi.pangaea.de/10.1594/PANGAEA.964672>  
577 and <https://doi.pangaea.de/10.1594/PANGAEA.964674>)

## 579 Author contributions

580 The study was designed by EM, MSP and KHB. EM and NMV carried out the morphometric measurements and classified the  
581 specimens of *E. huxleyi*. EM and MSP calculated coccolith-PICs, plotted the data and wrote an earlier version of the

manuscript. NB-J and HL provided remote sensing data for the study area, and were actively involved in the discussion of the findings as well as in the writing of the paper. All authors approved the submitted version.

## References

- Babin, M., Morel, A., Fournier-Sicre, V., Fell, F., and Stramski, D.: Light scattering properties of marine particles in coastal and open ocean waters as related to the particle mass concentration, *Limnology and Oceanography*, 48, 843-859, doi: 10.4319/lo.2003.48.2.0843, 2003a.
- Babin, M., Stramski, D., Ferrari, G. M., Claustre, H., Bricaud, A., Obolensky, G., and Hoepffner, N.: Variations in the light absorption coefficients of phytoplankton, nonalgal particles, and dissolved organic matter in coastal waters around Europe, *Journal of Geophysical Research: Oceans*, 108, doi: 10.1029/2001JC000882, 2003b.
- Bailey, S. W., & Werdell, P. J. (2006), A multi-sensor approach for the on-orbit validation of ocean color satellite data products, *Rem. Sens. Environ.*, 102, 12-23.
- Balch, W. M.: The Ecology, Biogeochemistry, and Optical Properties of Coccolithophores, *Annual Review of Marine Science*, 10, 71-98, doi: 10.1146/annurev-marine-121916-063319, 2018.
- Balch, W. M., Holligan, P. M., Ackleson, S. G., and Voss, K. J.: Biological and optical properties of mesoscale coccolithophore blooms in the Gulf of Maine, *Limnology and Oceanography*, 36, 629-643, doi: 10.4319/lo.1991.36.4.0629, 1991.
- Balch, W. M., Kilpatrick, K. A., Holligan, P., Harbour, D., and Fernandez, E.: The 1991 coccolithophore bloom in the central North Atlantic. 2. Relating optics to coccolith concentration, *Limnology and Oceanography*, 41, 1684-1696, 1996.
- Balch, W. M., Drapeau, D. T., Cucci, T. L., Vaillancourt, R. D., Kilpatrick, K. A., and Fritz, J. J.: Optical backscattering by calcifying algae: Separating the contribution of particulate inorganic and organic carbon fractions, *Journal of Geophysical Research: Oceans*, 104, 1541-1558, doi: 10.1029/1998JC900035, 1999.
- Balch, W. M., Gordon, H. R., Bowler, B. C., Drapeau, D. T., and Booth, E. S.: Calcium carbonate measurements in the surface global ocean based on Moderate-Resolution Imaging Spectroradiometer data, *Journal of Geophysical Research: Oceans*, 110, doi: 10.1029/2004JC002560, 2005.
- Balch, W. M., Drapeau, D. T., Bowler, B. C., Booth, E. S., Windecker, L. A., and Ashe, A.: Space-time variability of carbon standing stocks and fixation rates in the Gulf of Maine, along the GNATS transect between Portland, ME, USA, and Yarmouth, Nova Scotia, Canada, *Journal of Plankton Research*, 30, 119-139, doi: 10.1093/plankt/fbm097, 2007.
- Balch, W. M., Drapeau, D. T., Bowler, B. C., Lyczkowski, E., Booth, E. S., and Alley, D.: The contribution of coccolithophores to the optical and inorganic carbon budgets during the Southern Ocean Gas Exchange Experiment: New evidence in support of the “Great Calcite Belt” hypothesis, *Journal of Geophysical Research: Oceans*, 116, doi: 10.1029/2011jc006941, 2011.

612 Balch, W. M., Drapeau, D. T., Bowler, B. C., Lyczkowski, E. R., Lubelczyk, L. C., Painter, S. C., and Poulton, A. J.: Surface  
613 biological, chemical, and optical properties of the Patagonian Shelf coccolithophore bloom, the brightest waters of the  
614 Great Calcite Belt, *Limnology and Oceanography*, 59, 1715-1732, doi: 10.4319/lo.2014.59.5.1715, 2014.

615 Balch, W. M., Bates, N. R., Lam, P. J., Twining, B. S., Rosengard, S. Z., Bowler, B. C., Drapeau, D. T., Garley, R., Lubelczyk,  
616 L. C., Mitchell, C., and Rauschenberg, S.: Factors regulating the Great Calcite Belt in the Southern Ocean and its  
617 biogeochemical significance, *Global Biogeochemical Cycles*, 30, 1124-1144, doi: 10.1002/2016gb005414, 2016.

618 Balch, W. M., and Mitchell, C.: Remote sensing algorithms for particulate inorganic carbon (PIC) and the global cycle of PIC,  
619 *Earth-Science Reviews*, 239, 104363, doi: 10.1016/j.earscirev.2023.104363, 2023.

620 Balch, W. M., and P.E. Utgoff: Potential interactions among ocean acidification, coccolithophores, and the optical properties  
621 of seawater, *Oceanography and Marine Biology Annual Review*, 22, 146-159, doi: 10.5670/oceanog.2009.104, 2009.

622 Baumann, K.-H.: Importance of coccolith size measurements for carbonate estimations. *Micropaleontology*, 50 (1), 35-43,  
623 2004.

624 Beaufort, L.: Weight estimates of coccoliths using the optical properties (birefringence) of calcite, *Micropaleontology*, 51,  
625 289-298, 2005.

626 Beaufort, L., Probert, I., de Garidel-Thoron, T., Bendif, E. M., Ruiz-Pino, D., Metzl, N., Goyet, C., Buchet, N., Coupel, P.,  
627 Grelaud, M., Rost, B., Rickaby, R. E. M., and de Vargas, C.: Sensitivity of coccolithophores to carbonate chemistry and  
628 ocean acidification, *Nature*, 476, 80-83, doi: 10.1038/nature10295, 2011.

629 Bendif, E. M., Probert, I., Archontikis, O. A., Young, J. R., Beaufort, L., Rickaby, R. E., and Filatov, D.: Rapid diversification  
630 underlying the global dominance of a cosmopolitan phytoplankton, *The ISME Journal*, 17, 630-640, doi: 10.1038/s41396-  
631 023-01365-5, 2023.

632 Beuvier, T., Probert, I., Beaufort, L., Suchéras-Marx, B., Chushkin, Y., Zontone, F., and Gibaud, A.: X-ray nanotomography  
633 of coccolithophores reveals that coccolith mass and segment number correlate with grid size, *Nature Communications*,  
634 10, 751, doi: 10.1038/s41467-019-08635-x, 2019.

635 Bevington, P. R., *Data Reduction and Error Analysis for the Physical Sciences*, 336 pp., McGraw-Hill, 1969

636 Bi, S., Hieronymi, M., and Röttgers, R.: Bio-geo-optical modelling of natural waters, *Frontiers in Marine Science*, 10, doi:  
637 10.3389/fmars.2023.1196352, 2023.

638 Bollmann, J.: Technical Note: Weight approximation of coccoliths using a circular polarizer and interference colour derived  
639 retardation estimates - (The CPR Method), *Biogeosciences*, 11, 1899-1910, doi: 10.5194/bg-11-1899-2014, 2014.

640 Broerse, A. T. C., Tyrrell, T., Young, J. R., Poulton, A. J., Merico, A., Balch, W. M., and Miller, P. I.: The cause of bright  
641 waters in the Bering Sea in winter, *Continental Shelf Research*, 23, 1579-1596, doi: 10.1016/j.csr.2003.07.001, 2003.

642 Cárdenas, P., Lange, C. B., Vernet, M., Esper, O., Srain, B., Vorrath, M.-E., Ehrhardt, S., Müller, J., Kuhn, G., Arz, H. W.,  
643 Lembke-Jene, L., and Lamy, F.: Biogeochemical proxies and diatoms in surface sediments across the Drake Passage  
644 reflect oceanic domains and frontal systems in the region, *Progress in Oceanography*, doi: 10.1016/j.pocean.2018.10.004,  
645 2018.

Charalampopoulou, A., Poulton, A. J., Bakker, D. C. E., Lucas, M. I., Stinchcombe, M. C., and Tyrrell, T.: Environmental drivers of coccolithophore abundance and calcification across Drake Passage (Southern Ocean), *Biogeosciences*, 13, 5917-5935, doi:10.5194/bg-13-5917-2016, 2016.

Cook, S. S., Whittock, L., Wright, S. W., and Hallegraeff, G. M.: Photosynthetic pigment and genetic differences between two Southern Ocean morphotypes of *Emiliania huxleyi* (Haptophyta), *Journal of Phycology*, 47, 615-626, doi: 10.1111/j.1529-8817.2011.00992.x, 2011.

Costello, D. K., Carder, K. L., and Hou, W.: Aggregation of diatom bloom in a mesocosm: Bulk and individual particle optical measurements, *Deep Sea Research Part II: Topical Studies in Oceanography*, 42, 29-45, doi: 10.1016/0967-0645(95)00003-9, 1995.

Cros, L., Kleijne, A., Zeltner, A., Billard, C., and Young, J. R.: New examples of holococcolith-heterococcolith combination coccospheres and their implications for coccolithophorid biology, *Marine Micropaleontology*, 39, 1-34, doi: 10.1016/S0377-8398(00)00010-4, 2000.

Cubillos, J. C., Wright, S. W., Nash, G., de Salas, M. F., Griffiths, B., Tilbrook, B., Poisson, A., and Hallegraeff, G. M.: Calcification morphotypes of the coccolithophorid *Emiliania huxleyi* in the Southern Ocean: changes in 2001 to 2006 compared to historical data, *Marine Ecology Progress Series*, 348, 47-54, doi: 10.3354/meps07058, 2007.

Daniels, C. J., Tyrrell, T., Poulton, A. J., and Pettit, L.: The influence of lithogenic material on particulate inorganic carbon measurements of coccolithophores in the Bay of Biscay, *Limnology and Oceanography*, 57, 145-153, doi: 10.4319/lo.2012.57.1.0145, 2012.

de Baar, H. J. W., de Jong, J. T. M., Bakker, D. C. E., Loscher, B. M., Veth, C., Bathmann, U., and Smetacek, V.: Importance of iron for plankton blooms and carbon dioxide drawdown in the Southern Ocean, *Nature*, 373, 412-415, doi: 10.1038/373412a0, 1995.

Devred, E., Sathyendranath, S., Stuart, V., Maass, H., Ulloa, O., and Platt, T.: A two-component model of phytoplankton absorption in the open ocean: Theory and applications, *Journal of Geophysical Research: Oceans*, 111, doi: 10.1029/2005JC002880, 2006.

Díaz-Rosas, F., Alves-de-Souza, C., Alarcón, E., Menschel, E., González, H. E., Torres, R., and von Dassow, P.: Abundances and morphotypes of the coccolithophore *Emiliania huxleyi* in southern Patagonia compared to neighbouring oceans and Northern Hemisphere fjords, *Biogeosciences*, 18, 5465-5489, doi: 10.5194/bg-18-5465-2021, 2021.

Ferreira, A., Garcia, V. M. T., and Garcia, C. A. E.: Light absorption by phytoplankton, non-algal particles and dissolved organic matter at the Patagonia shelf-break in spring and summer, *Deep Sea Research Part I: Oceanographic Research Papers*, 56, 2162-2174, doi: 10.1016/j.dsr.2009.08.002, 2009.

Fuertes, M.-Á., Flores, J.-A., and Sierro, F. J.: The use of circularly polarized light for biometry, identification and estimation of mass of coccoliths, *Marine Micropaleontology*, 113, 44-55, doi: 10.1016/j.marmicro.2014.08.007, 2014.

GEBCO Compilation Group: GEBCO\_2022 Grid. Data set available online from the British Oceanographic Data Centre, Liverpool, UK. doi: 10.5285/e0f0bb80-ab44-2739-e053-6c86abc0289c, 2022.

680 Gordon, A. L., Molinelli, E., and Baker, T.: Large-scale relative dynamic topography of the Southern Ocean, *Journal of*  
681 *Geophysical Research: Oceans*, 83, 3023-3032, doi: 10.1029/JC083iC06p03023, 1978.

682 Gordon, H. R., Brown, O. B., Evans, R. H., Brown, J. W., Smith, R. C., Baker, K. S., and Clark, D. K.: A semianalytic radiance  
683 model of ocean color, *Journal of Geophysical Research: Atmospheres*, 93, 10909-10924, doi:  
684 10.1029/JD093iD09p10909, 1988.

685 Gordon, H. R., Boynton, G. C., Balch, W. M., Groom, S. B., Harbour, D. S., and Smyth, T. J.: Retrieval of coccolithophore  
686 calcite concentration from SeaWiFS Imagery, *Geophysical Research Letters*, 28, 1587-1590, doi:  
687 10.1029/2000GL012025, 2001.

688 Gravalosa, J. M., Flores, J.-A., Sierro, F. J., and Gersonde, R.: Sea surface distribution of coccolithophores in the eastern  
689 Pacific sector of the Southern Ocean (Bellingshausen and Amundsen Seas) during the late austral summer of 2001,  
690 *Marine Micropaleontology*, 69, 16-25, doi: 10.1016/j.marmicro.2007.11.006, 2008.

691 Guitián, J., Fuertes, M. Á., Flores, J. A., Hernández-Almeida, I., and Stoll, H.: Variation in calcification of *Reticulofenestra*  
692 coccoliths over the Oligocene–Early Miocene, *Biogeosciences*, 19, 5007-5019, doi: 10.5194/bg-19-5007-2022, 2022.

693 Hansen, F. C., Witte, H. J., and Passarge, J.: Grazing in the heterotrophic dinoflagellate *Oxyrrhis marina*: Size selectivity and  
694 preference for calcified *Emiliania huxleyi* cells., *Aquatic Microbial Biology*, 10, 307–313, 1996.

695 Harlay, J., Borges, A. V., Van Der Zee, C., Delille, B., Godoi, R. H. M., Schiettecatte, L. S., Roevros, N., Aerts, K., Lapernat,  
696 P. E., Rebreanu, L., Groom, S., Daro, M. H., Van Grieken, R., and Chou, L.: Biogeochemical study of a coccolithophore  
697 bloom in the northern Bay of Biscay (NE Atlantic Ocean) in June 2004, *Progress in Oceanography*, 86, 317-336, doi:  
698 10.1016/j.pocean.2010.04.029, 2010.

699 Harper, D. A. T.: *Numerical Palaeobiology*, John Wiley & Sons, 1999.

700 Holligan, P. M., Viollier, M., Harbour, D. S., Camus, P., and Champagne-Philippe, M.: Satellite and ship studies of  
701 coccolithophore production along a continental shelf edge, *Nature*, 304, 339-342, doi: 10.1038/304339a0, 1983.

702 Holligan, P. M., Fernández, E., Aiken, J., Balch, W. M., Boyd, P., Burkill, P. H., Finch, M., Groom, S. B., Malin, G., Muller,  
703 K., Purdie, D. A., Robinson, C., Trees, C. C., Turner, S. M., and van der Wal, P.: A biogeochemical study of the  
704 coccolithophore, *Emiliania huxleyi*, in the North Atlantic, *Global Biogeochemical Cycles*, 7, 879-900, doi:  
705 10.1029/93gb01731, 1993.

706 Holligan, P. M., Charalampopoulou, A., and Hutson, R.: Seasonal distributions of the coccolithophore, *Emiliania huxleyi*, and  
707 of particulate inorganic carbon in surface waters of the Scotia Sea, *Journal of Marine Systems*, 82, 195-205, doi:  
708 10.1016/j.jmarsys.2010.05.007, 2010.

709 Horigome, M. T., Ziveri, P., Grelaud, M., Baumann, K. H., Marino, G., and Mortyn, P. G.: Environmental controls on the  
710 *Emiliania huxleyi* calcite mass, *Biogeosciences*, 11, 2295-2308, doi: 10.5194/bg-11-2295-2014, 2014.

711 Iida, T., Saitoh, S. I., Miyamura, T., Toratani, M., Fukushima, H., and Shiga, N.: Temporal and spatial variability of  
712 coccolithophore blooms in the eastern Bering Sea, 1998-2001, *Progress in Oceanography*, 55, 165-175, doi:  
713 10.1016/S0079-6611(02)00076-9, 2002.

714 Kleijne, A.: Morphology, taxonomy and distribution of extant coccolithophores (calcareous nannoplankton), Ph.D., Vrije  
 715 Universiteit, Amsterdam, 321 pp., 1993.

716 Klinck, J., and Nowlin, W. D.: Antarctic Circumpolar Current, in: Encyclopedia of Ocean Sciences, edited by: Steele, J. H.,  
 717 Academic Press, Oxford, 151-159, 2001.

718 Krumhardt, K. M., Lovenduski, N. S., Long, M. C., Levy, M., Lindsay, K., Moore, J. K., and Nissen, C.: Coccolithophore  
 719 growth and calcification in an acidified ocean: Insights from Community Earth System Model simulations, Journal of  
 720 Advances in Modeling Earth Systems, doi: 10.1029/2018ms001483, 2019.

721 Lamy, F.: The Expedition PS97 of the Research Vessel POLARSTERN to the Drake Passage in 2016, edited by: Berichte zur  
 722 Polar- und Meeresforschung = Reports on polar and marine research, E. b. F. L. w. c. o. t. p., 167 pp., 2016.

723 Malinverno, E., Triantaphyllou, M. V., and Dimiza, M. D.: Coccolithophore assemblage distribution along a temperate to polar  
 724 gradient in the West Pacific sector of the Southern Ocean (January 2005) Micropaleontology, 61, 489-506 2015.

725 Malinverno, E., Maffioli, P., and Gariboldi, K.: Latitudinal distribution of extant fossilizable phytoplankton in the Southern  
 726 Ocean: Planktonic provinces, hydrographic fronts and palaeoecological perspectives, Marine Micropaleontology, 123,  
 727 41-58, doi: 10.1016/j.marmicro.2016.01.001, 2016.

728 Mitchell, C., Hu, C., Bowler, B., Drapeau, D., and Balch, W. M.: Estimating Particulate Inorganic Carbon Concentrations of  
 729 the Global Ocean From Ocean Color Measurements Using a Reflectance Difference Approach, Journal of Geophysical  
 730 Research: Oceans, 122, 8707-8720, doi: 10.1002/2017JC013146, 2017.

731 Mohan, R., Mergulhao, L. P., Guptha, M. V. S., Rajakumar, A., Thamban, M., AnilKumar, N., Sudhakar, M., and Ravindra,  
 732 R.: Ecology of coccolithophores in the Indian sector of the Southern Ocean, Marine Micropaleontology, 67, 30-45, doi:  
 733 10.1016/j.marmicro.2007.08.005, 2008.

734 Monteiro, F. M., Bach, L. T., Brownlee, C., Bown, P., Rickaby, R. E. M., Poulton, A. J., Tyrrell, T., Beaufort, L., Dutkiewicz,  
 735 S., Gibbs, S., Gutowska, M. A., Lee, R., Riebesell, U., Young, J., and Ridgwell, A.: Why marine phytoplankton calcify,  
 736 Science Advances, 2, e1501822, doi: doi:10.1126/sciadv.1501822, 2016.

737 NASA Goddard Space Flight Center, Ocean Ecology Laboratory, Ocean Biology Processing Group. Moderate-resolution  
 738 Imaging Spectroradiometer (MODIS) Aqua Level-2 Ocean Color, Version 2022 Data; NASA OB.DAAC, Greenbelt,  
 739 MD, USA. doi: 10.5067/AQUA/MODIS/L2/OC/2022, 2022a [Accessed on 10 July 2024].

740 NASA Goddard Space Flight Center, Ocean Ecology Laboratory, Ocean Biology Processing Group: Moderate-resolution  
 741 Imaging Spectroradiometer (MODIS) Aqua Level-3 Mapped Particulate Inorganic Carbon, Version 2022 Data; NASA  
 742 OB.DAAC, Greenbelt, MD, USA. doi: 10.5067/AQUA/MODIS/L3M/PIC/2022, 2022b [Access 01 June 2023].

743 NASA Ocean Biology Processing Group: Particulate Inorganic Carbon (PIC). Available from  
 744 <https://oceancolor.gsfc.nasa.gov/resources/atbd/pic/>, 2023 [Access 14 June 2023].

745 Neukermans, G., Oziel, L., and Babin, M.: Increased intrusion of warming Atlantic water leads to rapid expansion of temperate  
 746 phytoplankton in the Arctic, Global Change Biology, 24, 2545-2553, doi: 10.1111/gcb.14075, 2018.

Okada, H., and McIntyre, A.: Modern coccolithophores of the Pacific and North Atlantic oceans, *Micropaleontology*, 23, 1-54, doi: 10.2307/1485309 1977.

Oliver, H., McGillicuddy, D. J., J., Krumhardt, K. M., Long, M. C., Bates, N. R., Bowler, B. C., Drapeau, D. T., and Balch, W. M.: Environmental drivers of coccolithophore growth in the Pacific sector of the Southern Ocean, *Global Biogeochemical Cycles*, 37(11), <https://doi.org/10.1029/2023GB007751>, 2023.

Orsi, A. H., and Harris, U.: Fronts of the Antarctic Circumpolar Current - GIS data, Ver. 1, Australian Antarctic Data Centre - [https://data.aad.gov.au/metadata/records/antarctic\\_circumpolar\\_current\\_fronts](https://data.aad.gov.au/metadata/records/antarctic_circumpolar_current_fronts), 2019 [Access 26 May 2023].

Orsi, A. H., Whitworth III, T., and Nowlin Jr, W. D.: On the meridional extent and fronts of the Antarctic Circumpolar Current, *Deep Sea Research Part I: Oceanographic Research Papers*, 42, 641-673, doi: 10.1016/0967-0637(95)00021-w, 1995.

Poulton, A. J., Young, J. R., Bates, N. R., and Balch, W. M.: Biometry of detached *Emiliana huxleyi* coccoliths along the Patagonian Shelf, *Marine Ecology Progress Series*, 443, 1-17, doi: 10.3354/meps09445, 2011.

Poulton, A. J., Painter, S. C., Young, J. R., Bates, N. R., Bowler, B., Drapeau, D., Lyczskowski, E., and Balch, W. M.: The 2008 *Emiliana huxleyi* bloom along the Patagonian Shelf: Ecology, biogeochemistry, and cellular calcification, *Global Biogeochemical Cycles*, 27, 1023-1033, doi: 10.1002/2013GB004641, 2013.

Reynolds, R. A., Stramski, D., and Mitchell, B. G.: A chlorophyll-dependent semianalytical reflectance model derived from field measurements of absorption and backscattering coefficients within the Southern Ocean, *Journal of Geophysical Research: Oceans*, 106, 7125-7138, doi: 10.1029/1999JC000311, 2001.

Rigual Hernández, A. S., Flores, J. A., Sierro, F. J., Fuertes, M. A., Cros, L., and Trull, T. W.: Coccolithophore populations and their contribution to carbonate export during an annual cycle in the Australian sector of the Antarctic zone, *Biogeosciences*, 15, 1843-1862, BG, 2018.

Rigual Hernández, A. S., Trull, T. W., Nodder, S. D., Flores, J. A., Bostock, H., Abrantes, F., Eriksen, R. S., Sierro, F. J., Davies, D. M., Ballegeer, A. M., Fuertes, M. A., and Northcote, L. C.: Coccolithophore biodiversity controls carbonate export in the Southern Ocean, *Biogeosciences*, 17, 245-263, doi: 10.5194/bg-17-245-2020, 2020a.

Rigual-Hernández, A. S., Trull, T. W., Flores, J. A., Nodder, S. D., Eriksen, R., Davies, D. M., Hallegraeff, G. M., Sierro, F. J., Patil, S. M., Cortina, A., Ballegeer, A. M., Northcote, L. C., Abrantes, F., and Rufino, M. M.: Full annual monitoring of Subantarctic *Emiliana huxleyi* populations reveals highly calcified morphotypes in high-CO<sub>2</sub> winter conditions, *Scientific reports*, 10, 2594, doi: 10.1038/s41598-020-59375-8, 2020b.

Rivero-Calle, S., Gnanadesikan, A., Del Castillo, C. E., Balch, W. M., and Guikema, S. D.: Multidecadal increase in North Atlantic coccolithophores and the potential role of rising CO<sub>2</sub>, *Science*, 350, 1533-1537, doi: 10.1126/science.aaa8026, 2015.

Robertson, J. E., Robinson, C., Turner, D. R., Holligan, P., Watson, A. J., Boyd, P., Fernandez, E., & Finch, M. (1994), The impact of a coccolithophore bloom on oceanic carbon uptake in the northeast Atlantic during summer 1991, *Deep-Sea Research Part I*, 41(2), 297-314, doi:10.1016/0967-0637(94)90005-1.



780 Rost, B., and Riebesell, U.: Coccolithophore calcification and the biological pump: response to environmental changes, in:  
781 Coccolithophores: from molecular processes to global impact, edited by: Thierstein, H. R., and Young, J. R., Springer,  
782 Berlin-Heidelberg, Germany, 99-125, 2004.

783 Saavedra-Pellitero, M., Baumann, K.-H., Flores, J.-A., and Gersonde, R.: Biogeographic distribution of living  
784 coccolithophores in the Pacific sector of the Southern Ocean, *Marine Micropaleontology*, 109, 1-20, doi:  
785 10.1016/j.marmicro.2014.03.003, 2014.

786 Saavedra-Pellitero, M., Baumann, K. H., Fuertes, M. Á., Schulz, H., Marcon, Y., Vollmar, N. M., Flores, J. A., and Lamy, F.:  
787 Calcification and latitudinal distribution of extant coccolithophores across the Drake Passage during late austral summer  
788 2016, *Biogeosciences*, 16, 3679-3702, doi: 10.5194/bg-16-3679-2019, 2019.

789 Salter, I., Schiebel, R., Ziveri, P., Movellan, A., Lampitt, R., and Wolff, G. A.: Carbonate counter pump stimulated by natural  
790 iron fertilization in the Polar Frontal Zone, *Nature Geoscience*, 7, 885-889, doi: 10.1038/ngeo2285, 2014.

791 Samtleben, C. and Schröder, A.: Living coccolithophore communities in the Norwegian-Greenland Sea and their record in  
792 sediments, *Marine Micropaleontology*, 19, 333-354, 1992.

793 Schindelin, J., Arganda-Carreras, I., Frise, E., Kaynig, V., Longair, M., Pietzsch, T., Preibisch, S., Rueden, C., Saalfeld, S.,  
794 Schmid, B., Tinevez, J.-Y., White, D. J., Hartenstein, V., Eliceiri, K., Tomancak, P., and Cardona, A.: Fiji: an open-  
795 source platform for biological-image analysis, *Nature Methods*, 9, 676-682, doi: 10.1038/nmeth.2019, 2012.

796 Schneider, C. A., Rasband, W. S., and Eliceiri, K. W.: NIH Image to ImageJ: 25 years of image analysis, *Nature Methods*, 9,  
797 671-675, doi: 10.1038/nmeth.2089, 2012.

798 Shutler, J. D., Land, P. E., Brown, C. W., Findlay, H. S., Donlon, C. J., Medland, M., Snooke, R., and Blackford, J. C.:  
799 Coccolithophore surface distributions in the North Atlantic and their modulation of the air-sea flux of CO<sub>2</sub> from 10 years  
800 of satellite Earth observation data, *Biogeosciences*, 10, 2699-2709, doi: 10.5194/bg-10-2699-2013, 2013.

801 Siegel, H., Ohde, T., Gerth, M., Lavik, G., and Leipe, T.: Identification of coccolithophore blooms in the SE Atlantic Ocean  
802 off Namibia by satellites and in-situ methods, *Continental Shelf Research*, 27, 258-274, doi: 10.1016/j.csr.2006.10.003,  
803 2007.

804 Smyth, T. J., Moore, G. F., Groom, S. B., Land, P. E., and Tyrrell, T.: Optical modeling and measurements of a coccolithophore  
805 bloom, *Appl. Opt.*, 41, 7679-7688, doi: 10.1364/AO.41.007679, 2002.

806 Smyth, T. J., Tyrrell, T., and Tarrant, B.: Time series of coccolithophore activity in the Barents Sea, from twenty years of  
807 satellite imagery, *Geophysical Research Letters*, 31, doi: 10.1029/2004GL019735, 2004.

808 Suchéras-Marx, B., Viseur, S., Walker, C. E., Beaufort, L., Probert, I., and Bolton, C.: Coccolith size rules – What controls  
809 the size of coccoliths during coccolithogenesis?, *Marine Micropaleontology*, 170, 102080, doi:  
810 10.1016/j.marmicro.2021.102080, 2022.

811 Trull, T. W., Passmore, A., Davies, D. M., Smit, T., Berry, K., and Tilbrook, B.: Distribution of planktonic biogenic carbonate  
812 organisms in the Southern Ocean south of Australia: a baseline for ocean acidification impact assessment,  
813 *Biogeosciences*, 15, 31-49, doi: 10.5194/bg-15-31-2018, 2018.

814 Tyrrell, T., and Taylor, A. H.: A modelling study of *Emiliana huxleyi* in the NE atlantic, Journal of Marine Systems, 9, 83-  
815 112, doi:10.1016/0924-7963(96)00019-X, 1996.

816 Vollmar, N. M., Baumann, K.-H., Saavedra-Pellitero, M., and Hernández-Almeida, I.: Distribution of coccoliths in surface  
817 sediments across the Drake Passage and calcification of *Emiliana huxleyi* morphotypes, Biogeosciences, 19, 585–612,  
818 <https://doi.org/10.5194/bg-19-585-2022>, 2022.

819 von Dassow, P., Díaz-Rosas, F., Bendif, E. M., Gaitán-Espitia, J. D., Mella-Flores, D., Rokitta, S., John, U., and Torres, R.:  
820 Over-calcified forms of the coccolithophore *Emiliana huxleyi* in high-CO<sub>2</sub> waters are not preadapted to ocean  
821 acidification, Biogeosciences, 15, 1515-1534, doi: 10.5194/bg-15-1515-2018, 2018.

822 Werdell, J., O'Reilly, J., Hu, C., Feng, L., Lee, Z., Franz, B., Bailey, S., Proctor, C., and Wang, G.: Chlorophyll a. NASA  
823 Algorithm Publication Tool, 2023-11-06, v1.1. Available from <https://www.earthdata.nasa.gov/documents/chlor-a/v1.1>,  
824 2023, <https://doi.org/10.5067/JCQB8QALDOYD> [Access 20 July 2024]

825 Whitworth, T. I.: Zonation and geostrophic flow of the Antarctic circumpolar current at Drake Passage, Deep Sea Research  
826 Part A. Oceanographic Research Papers, 27, 497-507, doi: 10.1016/0198-0149(80)90036-9, 1980.

827 Winter, A., Elbrächter, M., and Krause, G.: Subtropical coccolithophores in the Weddell Sea, Deep Sea Research Part I:  
828 Oceanographic Research Papers, 46, 439-449, doi: 10.1016/S0967-0637(98)00076-4, 1999.

829 Winter, A., Henderiks, J., Beaufort, L., Rickaby, R. E. M., and Brown, C. W.: Poleward expansion of the coccolithophore  
830 *Emiliana huxleyi*, Journal of Plankton Research, 36, 316-325, 10.1093/plankt/fbt110, 2014.

831 Yang, T. N., and Wei, K. Y.: How many coccoliths are there in a coccosphere of the extant coccolithophorids? A compilation,  
832 Journal of Nannoplankton Research, 25, 7-15, 2003.

833 Young, J.: Coccobiom2 Macros, available from: <http://ina.tmsoc.org/nannos/coccobiom/Usernotes.html>, 2015 [Access 23  
834 August 2017]

835 Young, J. R., and Ziveri, P.: Calculation of coccolith volume and it use in calibration of carbonate flux estimates, Deep Sea  
836 Research Part II: Topical Studies in Oceanography, 47, 1679-1700, doi: 10.1016/S0967-0645(00)00003-5, 2000.

837 Young, J. R., Poulton, A. J., and Tyrrell, T.: Morphology of *Emiliana huxleyi* coccoliths on the northwestern European shelf  
838 – is there an influence of carbonate chemistry?, Biogeosciences, 11, 4771-4782, doi: 10.5194/bg-11-4771-2014, 2014.

839

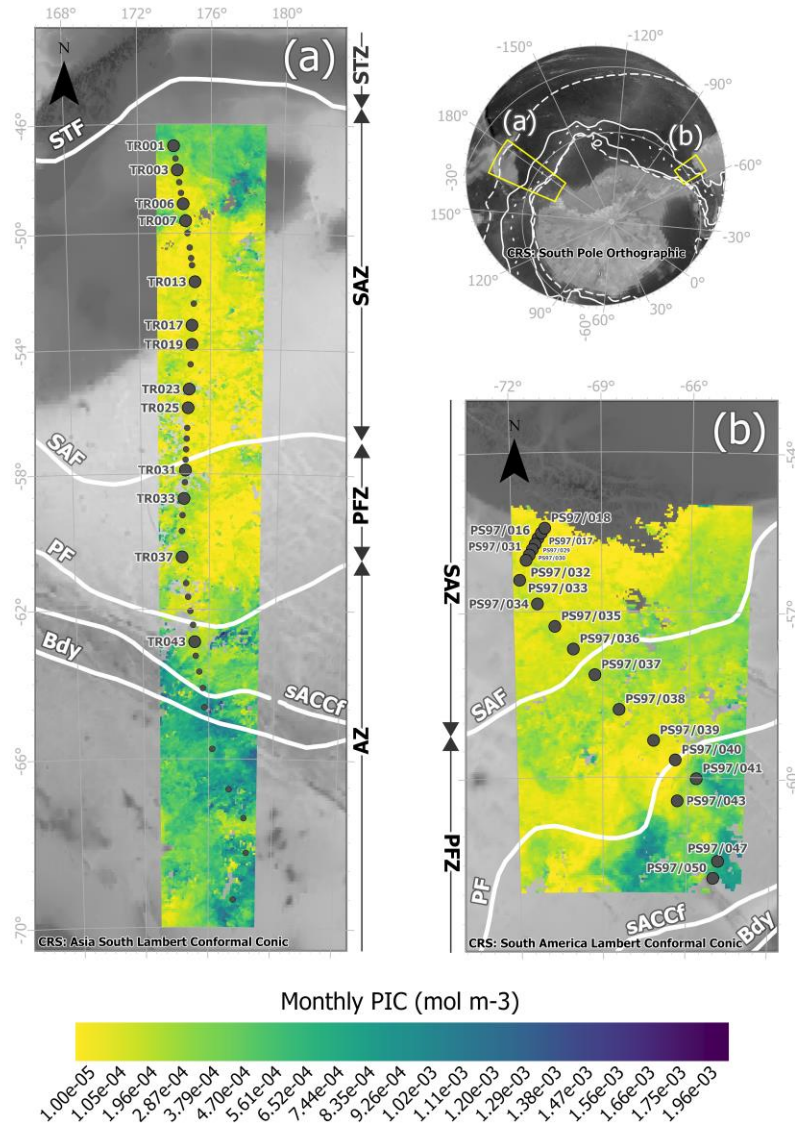


**Figure 1: Study area showing the location of the water samples retrieved from (a) the New Zealand transect, collected during the XX Italian Expedition from New Zealand to Antarctica on board R/V *Italica* (December 2004-January 2005) and (b) the Drake Passage transect, collected during *Polarstern* Expedition PS97 across the Drake Passage (February-March 2016). Large dots indicate samples in which biometries on *Emiliana huxleyi* were performed, and small dots where coccolithophore census were available. The maps show MODIS-Aqua L3 PIC concentrations in mol m<sup>-3</sup> g corresponding to (a) monthly mean over January 2005 and (b) monthly mean over February and March 2016, overlain on a bathymetry background (GEBCO Compilation Group, 2022). White lines indicate the average position of the ACC fronts (Orsi and Harris, 2019), from north to south these are: SAF (Subantarctic Front), PF (Polar Front), sACCF (Southern ACC Front) and Bdy (Southern Boundary). The Southern Ocean zones are labeled on the side of each map: STZ, Subtropical Zone; SAZ, Subantarctic Zone; PFZ, Polar Frontal Zone; AZ, Antarctic Zone.**

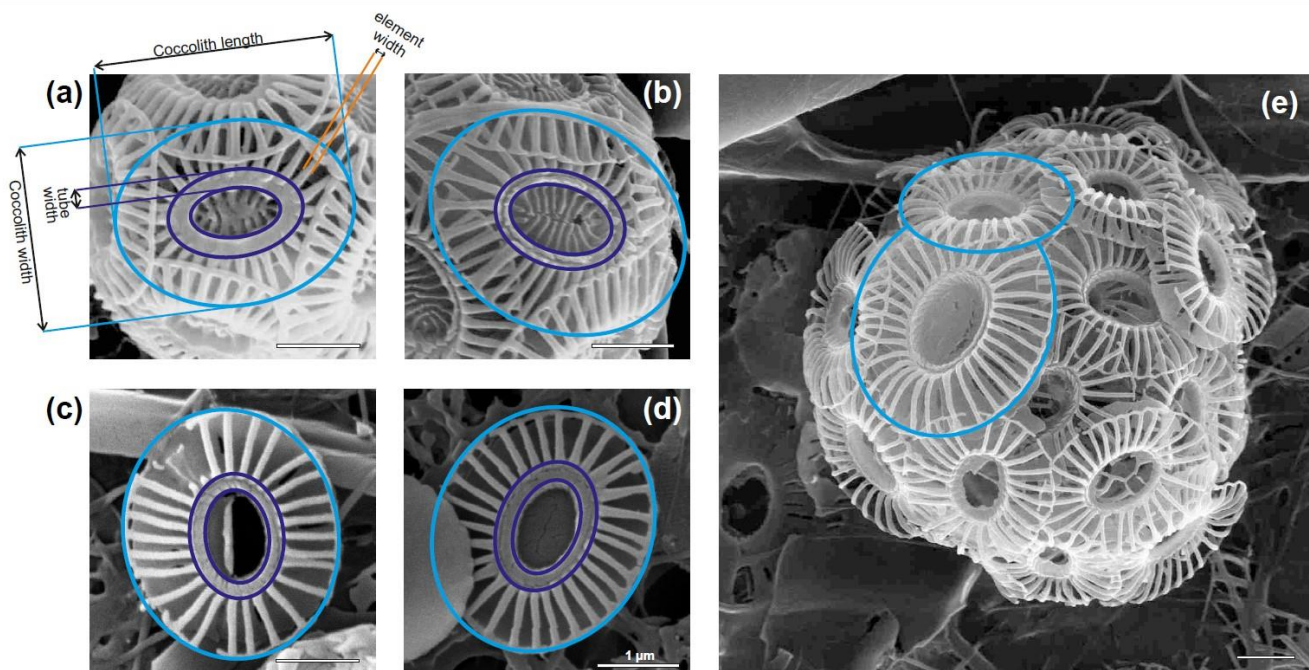
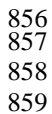


**Figure 2: Parameters measured in *Emiliana huxleyi* coccoliths (a, b) type A and (c, d, e) type O in plankton samples from the New Zealand transect. Note the coccolith size variation in (e) within the same coccosphere.**



29

with diamonds), weekly average (light blue dashed line with crosses), (c) MODIS-Aqua L2 PIC concentration values in  $\text{mol m}^{-3}$  (average in pink) (d) *Emiliania huxleyi* relative tube width index (average in gray), (e) *E. huxleyi* coccolith mass estimates (pg) for morphogroup A (dots) and B (circles) (average in gray), (f) number of bilayered *E. huxleyi* (coccospheres/L), (g) number of *E. huxleyi* morphogroup A (coccospheres/L), (h) number of *E. huxleyi* morphogroup B (coccospheres/L), (i) number of *Calcidiscus leptoporus* (coccospheres/L), (j) Number of total coccolithophores (coccospheres/L) (Malinverno et al., 2015), (k) Number of total diatoms (cells/L) (Malinverno et al., 2016), (l) MODIS-Aqua L2 chlorophyll a concentration in  $\text{mg m}^{-3}$  (average in light green). Note that the plankton samples were retrieved at ca. 3 m water depth. Vertical bars indicate one standard deviation on the entire population in (a), (d) and (e), and the standard deviation (considering a 5 x 5 window) in (c) and (l). The shaded area in (a) represents a 50% error. Vertical dashed lines indicate some of the ACC fronts (Orsi and Harris, 2019): SAF (Subantarctic Front), PF (Polar Front) and sACCf (Southern ACC Front). The Southern Ocean zones are labeled as SAZ (Subantarctic Zone), PFZ (Polar Frontal Zone) and AZ (Antarctic Zone).

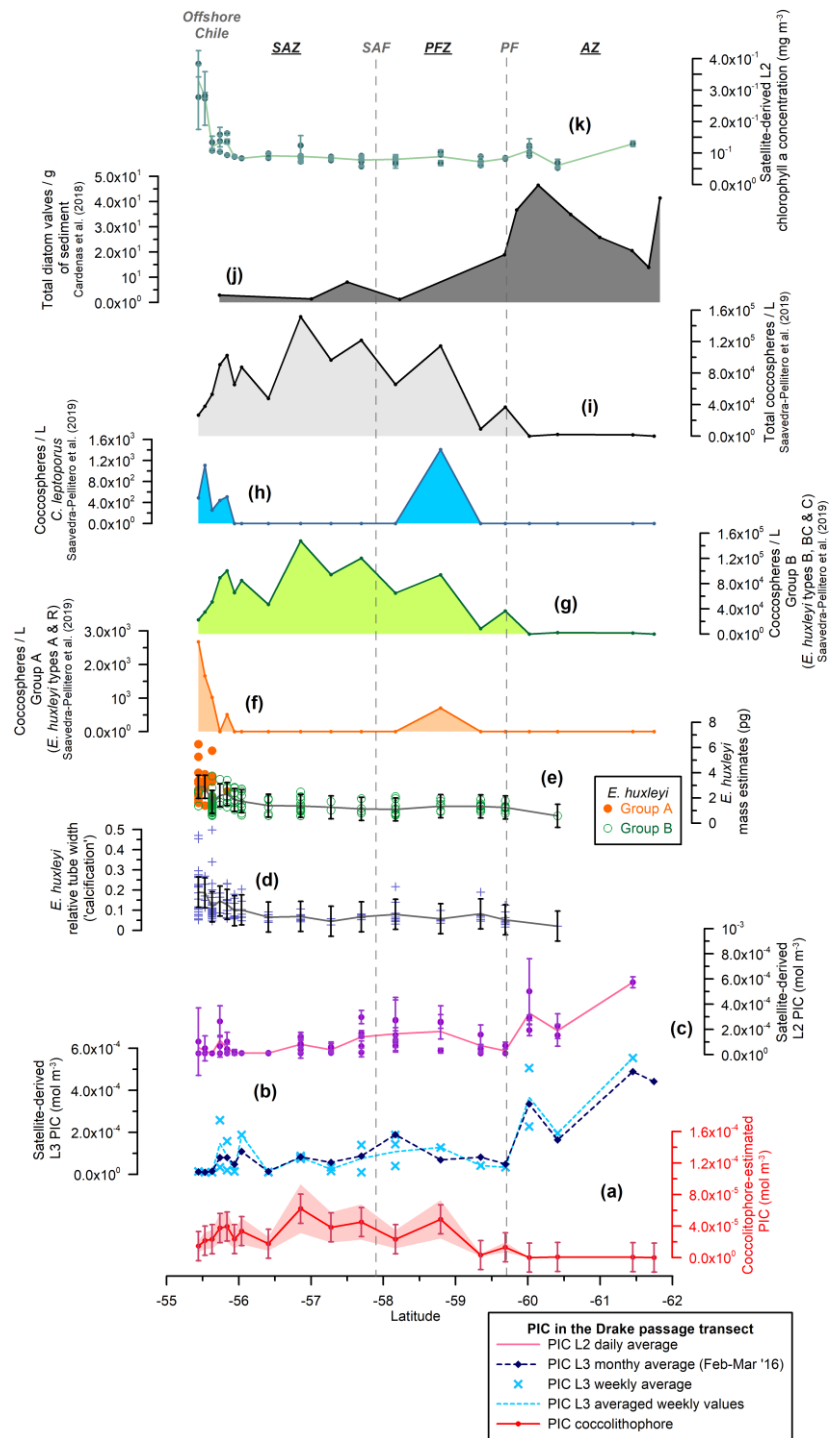
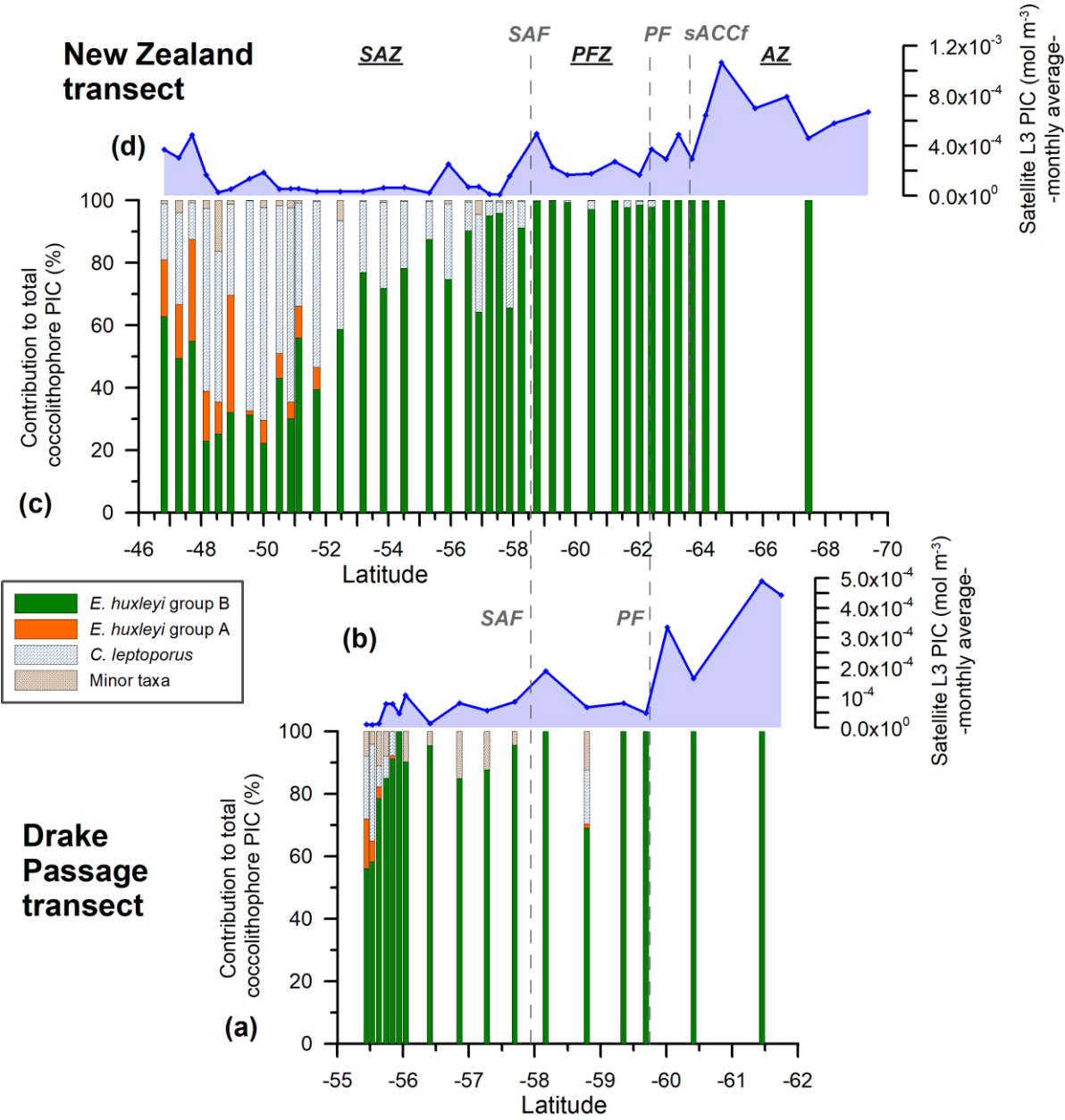


Figure 4: Drake Passage transect showing (a) estimated total coccolithophore PIC (red line with dots) in  $\text{mol m}^{-3}$ , (b) MODIS-Aqua L3 PIC concentration ( $\text{mol m}^{-3}$ ) corresponding to a monthly average (February and March 2016, dark blue dashed line with diamonds), weekly average (light blue dashed line with crosses), (c) MODIS-Aqua L2 PIC concentration in  $\text{mol m}^{-3}$  (average in

pink), (d) *Emiliana huxleyi* relative tube width index (average in gray), (e) *E. huxleyi* coccolith mass estimates (pg) for morphogroup A (dots) and B (circles) in (average in gray), (f) number of *E. huxleyi* morphogroup A (coccospheres/L), (g) number of *E. huxleyi* morphogroup B (coccospheres/L), (h) number of *Calcidiscus leptoporus* (coccospheres/L), (i) Number of total coccolithophores (coccospheres/L) (Saavedra-Pellitero et al., 2019), (j) Number of valves per gram of sediment from surface sediment samples across the Drake Passage and Scotia Sea (Cárdenas et al., 2018), (k) MODIS-Aqua L2 chlorophyll a concentration in  $\text{mg m}^{-3}$  (average in light green). Note that plankton samples were retrieved at 5, 10 and 20 m water depth. Vertical bars indicate one standard deviation on the entire population in (a), (d) and (e), and the standard deviation (considering a 5 x 5 window) in (c) and (k). The shaded area in (a) represents a 50% error. Vertical dashed lines indicate some of the ACC fronts (Orsi and Harris, 2019): SAF (Subantarctic Front) and PF (Polar Front). The Southern Ocean zones are labeled as SAZ (Subantarctic Zone), PFZ (Polar Frontal Zone) and AZ (Antarctic Zone).

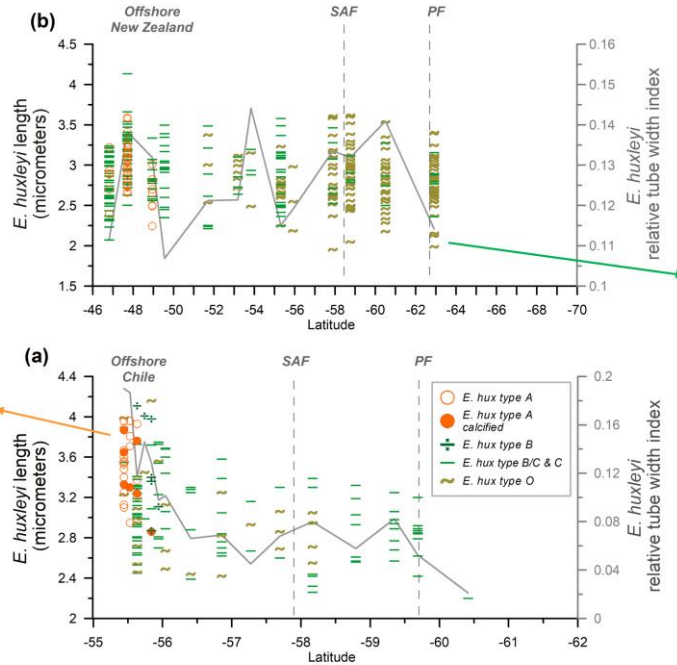
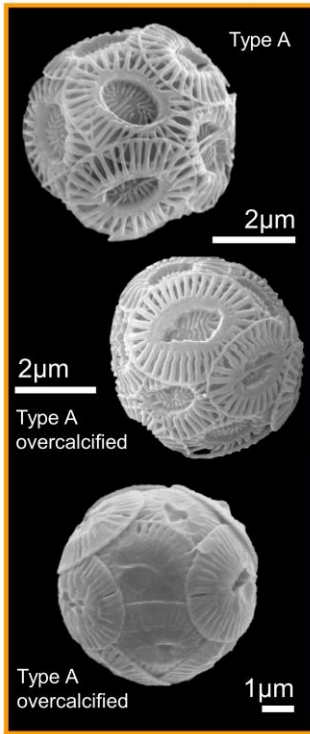




890  
891  
892  
893  
894  
895  
896  
897  
898  
899

**Figure 5:** New Zealand (NZ) and Drake Passage (DP) transects showing (a, c) the relative PIC contribution of the different nanofloral taxa (*E. huxleyi* morphogroups A and B, *Calcidiscus leptoporus* and minor species) to the estimated coccolithophore PIC in 38 NZ and 17 DP samples bearing coccospheres; (b, d) MODIS-Aqua L3 monthly average satellite-derived PIC values (February and March 2016, dark blue line with diamonds) in mol m<sup>-3</sup>. Vertical dashed lines indicate some of the ACC fronts (Orsi and Harris, 2019): SAF (Subantarctic Front) and PF (Polar Front). The Southern Ocean zones are labeled as SAZ (Subantarctic Zone), PFZ (Polar Frontal Zone) and AZ (Antarctic Zone).

## *E. huxleyi* morphogroup A



## *E. huxleyi* morphogroup B

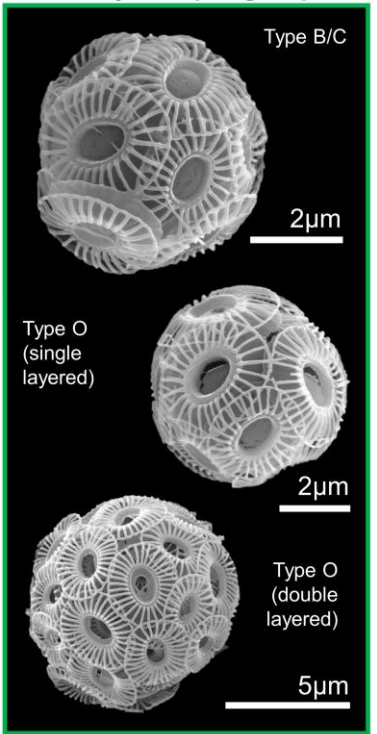
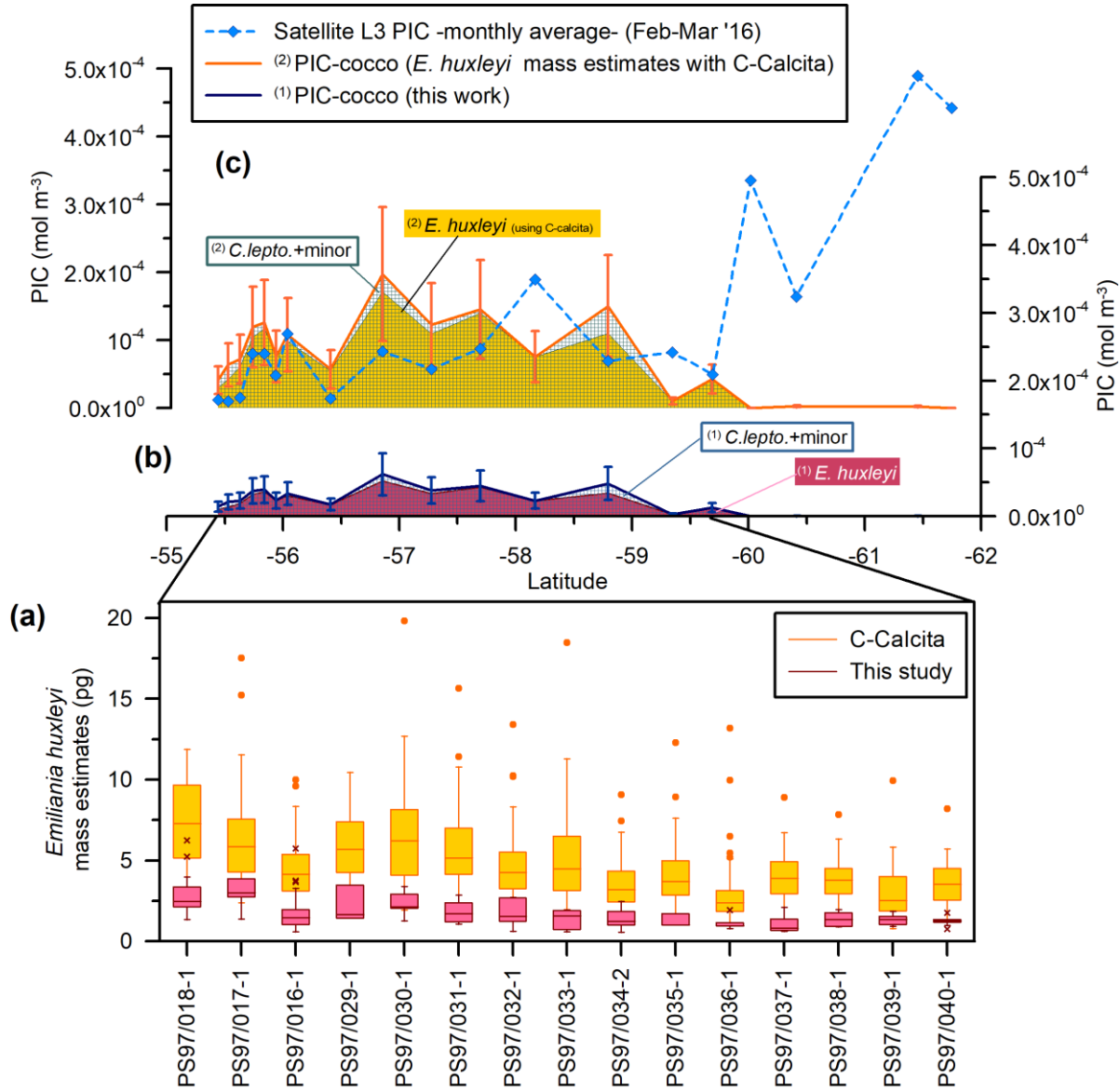


**Figure 6:** *Emiliana huxleyi* length (in  $\mu\text{m}$ ) (indicated with different symbols depending on the type, and different colors depending on the morphogroup A or B-) and averaged relative tube width index (gray line) in (a) the Drake Passage and (b) New Zealand transects. On the left-hand side: pictures of coccospheres of *E. huxleyi* type A (within the morphogroup A) showing different degrees of calcification and on the right-hand side pictures of type B/C as well as type O belonging to the morphogroup B. All the images of coccospheres are from the New Zealand transect, except for the left bottom one, which was retrieved offshore of Chile.

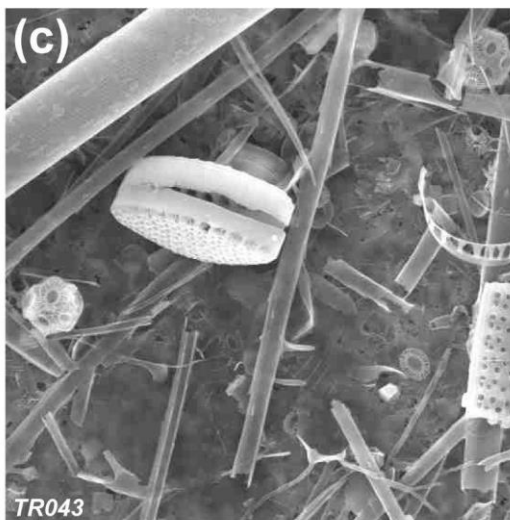
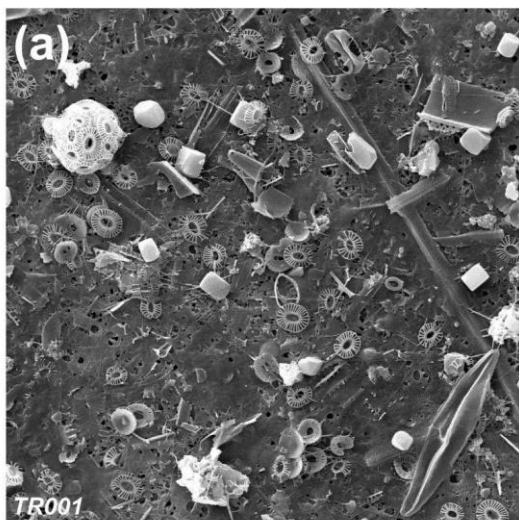
908  
909



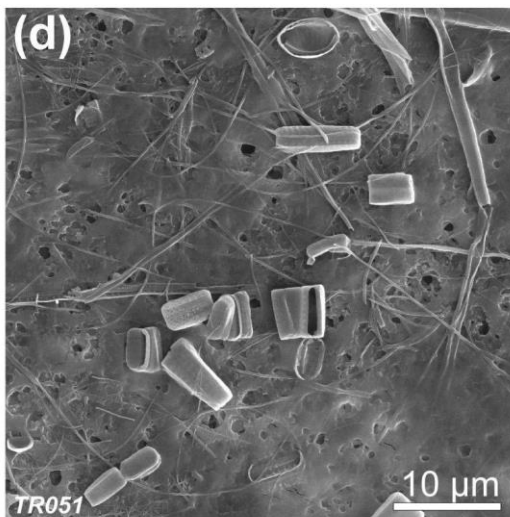
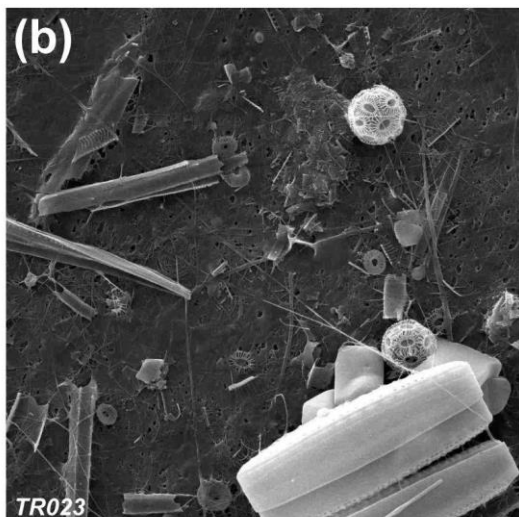
910  
911  
912  
913  
914  
915  
916  
917  
918  
919  
920

**Figure 7: Drake Passage latitudinal transect showing (a) coccolith mass estimates box plots (in pg): in dark red plus pink for this study (outliers are indicated with “x”) and yellow plus orange for Saavedra-Pellitero et al. (2019) (outliers are indicated with a dot); (b) estimated coccolithophore PIC (PIC-cocco) (all in  $\text{mol m}^{-3}$ ) -this study<sup>(1)</sup>;- (c) MODIS-Aqua L3 monthly average satellite-derived PIC values (blue dashed line with diamonds) and PIC-cocco calculated considering averaged *Emiliania huxleyi* mass estimates obtained with the software C-Calcita<sup>(2)</sup> (Saavedra-Pellitero et al., 2019). Note that the contributions of different coccolith taxa or groups have been indicated (*C.lepto.* = *Calcidiscus leptoporus*; minor = minor species) and that the data is stacked for each of the approaches. Vertical bars in (b) and (c) represent a 50% error.**

North  
-New  
Zealand-



North



South  
-Antarctica-

**Figure 8: SEM pictures of samples retrieved in the Subantactic Zone (a, b) and south of the Polar Front (c, d) in the New Zealand transect.**

926  
927  
928  
929

**Table 1: Overview of the samples considered for this study, including the sampling area, number of plankton samples considered for this study, expedition, research vessel, water sampling dates, coordinates and data already available from previous publications.**

Area	Number of samples considered for this work	Water depth (m)	Expedition	Research Vessel	Plankton sampling period	Coordinates	Previous publications
New Zealand	42	3	XX Italian Expedition	R/V Italica	31.12.2004-06.01.2005	46.81°S to 69.98°S	Coccolithophore assemblages: Malinverno et al. (2015); Dinoflagellates, Coccolithophores, Silicoflagellates, Diatoms, Parmales, Archaeomonads and micro-zooplankton: Malinverno et al. (2016)
Drake Passage	19	5, 10 and 20	Expedition PS97	Polarstern	24.02.2016-05.03.2016	55.44°S to 61.75°S	Coccolithophore assemblages: Saavedra-Pellitero et al. (2019); <i>Emiliana huxleyi</i> mass estimantes: Saavedra-Pellitero et al. (2019)

930  
931

**Table 2: Length, shape factors (Ks) and number of coccoliths per coccosphere used in this work for the New Zealand transect and the Drake Passage transect. (\*) Indicates an average of the number of coccoliths per coccosphere. Note that the different Ks used here were mostly based on Young and Ziveri (2000). The shape factor for morphotype O (Ks = 0.015) was introduced by Poulton et al. (2011) in a plankton study along the Patagonian Shelf for a morphotype with a central area described as an “open or thin plate” which the authors called type B/C but that we identified as morphotype O.**

Coccolithophore species	Average length ± standard deviation (µm) New Zealand	Average length ± standard deviation (µm) Drake Passage	Source	Ks	Source	Number of coccoliths per coccosphere N. Zealand	Number of coccoliths per coccosphere Drake P.	Source
<i>Calcidiscus leptoporus</i> spp. <i>leptoporus</i>	5.7±0.6	5.7±0.6	This work (biometries offshore N. Zealand)	0.08	Young and Ziveri (2000)	15	15	Kleijne (1993)
<i>Emiliania huxleyi</i> group A (average value)	2.95±0.28	3.49±0.33	This work	0.03	This work	15 single layered, 35 double layered	25 (*)	This work (own observations)
<i>Emiliania huxleyi</i> A overcalcified				0.04	Young and Ziveri (2000)			
<i>Emiliania huxleyi</i> A (normal)				0.02	Young and Ziveri (2000)			
<i>Emiliania huxleyi</i> group B (average value)	2.87±0.35	2.98±0.40	This work	0.02	Young and Ziveri (2000)			
<i>Emiliania huxleyi</i> B-B/C-C				0.02	Young and Ziveri (2000)			
<i>Emiliania huxleyi</i> O				0.015	Poulton et al. (2011)			
<i>Gephyrocapsa muelleriae</i>	3.9	3.9	Young and Ziveri (2000)	0.05	Young and Ziveri (2000)	15	15	Samtleben & Schroder (1992)
<i>Syracosphaera</i> spp.	2.2	5.5	Young and Ziveri (2000)	0.03	Young and Ziveri (2000)	25	25	Okada & McIntyre (1977)
Minor taxa			Young and Ziveri (2000)		Young and Ziveri (2000)			Yang & Wei (2003)



943  
944  
945  
946  
947  
948

**Table 3. Summary of MODIS-Aqua products used in this study.** <sup>(\*\*\*)</sup>The first 8-day period of each year always begins with January 1, the second with January 9, the third with January 17, etc. The final "8-day" composite of each year comprises only five days in non-leap years (27 - 31 December) or six days in leap years (26 - 31 December) (NASA Ocean Biology Processing Group, 2018).

				Drake passage transect		New Zealand transect	
<i>Satellite product</i>	<i>Biophysical variable</i>	<i>Extraction method</i>	<i>Time period</i>	<i>Time span</i>	<i>Num. of scenes</i>	<i>Time span</i>	<i>Num. of scenes</i>
MODIS-A Level 2	■ PIC concentration (mol m <sup>-3</sup> )	mean of 5x5 window centered on measurement location	Daily timestamp	17-02-2016 / 12-03-2016	50	24-12-2004 / 13-01-2005	34
	■ Chlorophyll a concentration (mg m <sup>-3</sup> )						
MODIS-A Level 3	PIC concentration (mol m <sup>-3</sup> )	value of pixel enclosing measurement location	8-daily <sup>(**)</sup> timestamp	10-02-2016 / 12-03-2016	4	26-12-2004 / 08/01/2005	2
MODIS-A Level 3	PIC concentration (mol m <sup>-3</sup> )	value of pixel enclosing measurement location	Monthly timestamp	01-12-2004 / 31/01/2005	2	01-02-2016 / 31/03/2016	2

949  
950  
951  
952  
953  
954